



國立臺灣大學電機資訊學院電機工程學研究所

碩士論文

Graduate Institute of Electrical Engineering

College of Electrical Engineering and Computer Science

National Taiwan University

Master Thesis

第五代毫米波通訊系統下指向性參考信號設計

與排程機制

Directional Reference Signal Design and

Scheduling Mechanism for 5G Millimeter Wave

Cellular Systems

翁仲威

Chung-Wei Weng

指導教授：魏宏宇博士

Advisor: Hung-Yu Wei, Ph.D.

中華民國 105 年 7 月

July, 2016



誌謝

感謝魏宏宇老師細心且耐心的指導，使我這篇論文得以完成。感謝所有口試的評鑑委員：蔡欣穆教授、周俊廷教授與王志宇博士，你們的建議使這篇論文更加完善。感謝聯發科的游家豪博士與易志熹博士，兩年來的臺大聯發科產學大聯盟計畫給我諸多研究上的建議。感謝實驗室的同伴們，感謝駿彥學長在我研究的初始階段指點我許多地方，感謝冠宇學長常回答我的一些疑惑，感謝 Biswa 在英文寫作技巧上給我建議。一起度過兩年的我的快樂小夥伴們：張翼、廷華、凱程，不論是修課時期末專題的協作，或是平時討論研究上對我的一些啟發，都惠我良多。感謝開源社的社胞伴我兩年，為我的研究生活帶來歡樂。最重要的是感謝我的父母的支持與陪伴。今日我能完成碩士學業，稍有所成非一己之力得感謝的人繁多不能一一提起，感謝你們才有今日的我。



摘要

毫米波頻帶提供了一個可以支援數億位元傳輸率的新未開發頻帶給無線行動通訊系統。但是毫米波頻帶的通道傳輸物理特性比一般低頻的電波還要脆弱，因此必須使用指向性天線將能量集中在傳輸方向形成波束克服。指向性天線在無線行動通訊系統的使用面臨許多嶄新的挑戰，例如指向性參考信號的設計。指向性參考信號可用作量測通道品質、波束追蹤與裝置移動性管理。在本篇論文中，設計指向性參考信號使之確保整個基地台的參考信號覆蓋範圍且提升參考信號在行動裝置端的頻繁接收率。並且利用指向性參考信號的特性，設計出兼具行動裝置省電與高傳輸流量的排程機制。在這篇論文中透過數學理論分析與電腦數值模擬結果驗證了提出方法比起傳統方法的突出表現。



Abstract

Millimeter wave (mmWave) frequency bands offer a new frontier for cellular wireless systems to enable multigigabit communication. However, the availability and reliability of mmWave links are significantly limited due to its propagation characteristics. To mitigate the impact of such links and provide uninterrupted network services, the study of changing link condition is important. This paper proposes a reference signal (RS) transmission scheme and RS aware scheduling mechanism for a mmWave cellular system using highly directional antenna beams. The aim of RS is to estimate the channel condition which can be used for various purposes, e.g. initial access, beam alignment, and channel state information (CSI) measurement. In particular, the objective of our RS scheme is to enable efficient RS transmission in terms of RS frequently reception while ensuring a fair number of RS reception at all UEs within cell coverage. In addition, we provide a scheduling mechanism considering directional RS for studying the system throughput. Through theoretical analysis and simulation, we show that the proposed scheme achieves higher efficiency.



Contents

誌謝	i
摘要	ii
Abstract	iii
1 Introduction	1
2 Directional Reference Signal Design for 5G Millimeter Wave Cellular Systems	5
2.1 Introduction	5
2.2 Related Work	6
2.3 Overview of Proposed Scheme	8
2.3.1 Working Principle	8
2.3.2 Frame Format of Reference Signal	9
2.3.3 Full Reference Signal Transmission Period	11
2.3.4 Efficient Reference Signal Transmission Period	11
2.3.5 Reference Signal Measurements	12
2.4 System Model	15
2.4.1 Network Model	15
2.4.2 Channel Model	16

2.4.3	Mathematical Formulation	17
2.5	Performance Evaluation and Analysis	22
2.6	Summary	29
3	Scheduling Mechanism for 5G Millimeter Wave Cellular Systems	32
3.1	Introduction	32
3.2	Related Work	33
3.3	System Model	34
3.4	Proposed Scheduling Mechanism	34
3.5	Simulator	38
3.6	Evaluation and Results	40
3.7	Summary	46
4	Conclusion	48
	Bibliography	49

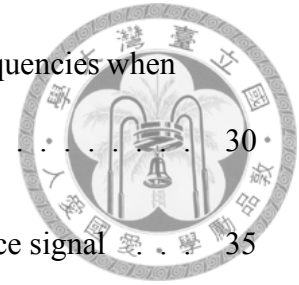




List of Figures

1.1	(a) Beam coverage at different frequency band using sector and narrow beam, (b) Narrow beam transmitted with full-power, (c) Total transmission power is shared among multiple narrow beams result in smaller coverage.	3
2.1	Illustration of Proposed Reference Signaling Scheme	9
2.2	Frame format of Reference Signal	10
2.3	Proposed Reference Signaling Flow	14
2.4	The mmWave network model used in this work.	15
2.5	The number of RS received at each UE per time slot varying Efficient-RSTP cycles and $\mathcal{N}_b = \{2, 3, 4, 6\}$	24
2.6	The cumulative distribution function (CDF) of RS received per time slot for different SP cycles.	25
2.7	Performance comparison of three different schemes. $\mathcal{N}_b = 2$, $\mathcal{C}_s = 2$ and $\mathcal{C}_e = 3$	26
2.8	The number of RS received per time slot for different number of simultaneous beam in SP varying number of UEs. Here, we set $\eta = 3$ and $\mathcal{T}_{Max} = 600$	28

2.9	Performance variation due to different mmWave carrier frequencies when number of UE $n = 75$, $\eta = 3$, and $\mathcal{T}_{Max} = 600$	30
3.1	illustration for UE power state transition right after reference signal	35
3.2	An example of scheduling data transmission for schedulable time = 4 slots	36
3.3	BS antenna Gain pattern	39
3.4	BS antenna field pattern gain magnitude at each directional beam	40
3.5	UE antenna field pattern gain magnitude at each beam	41
3.6	Throughput component in each slot contribute to system throughput for different schedulable time duration	43
3.7	Throughput versus schedulable time when UE velocity is 5 km/hr	44
3.8	Throughput versus UE velocity	44
3.9	Throughput component in each slot contribute to system throughput for different schedulable time duration	45
3.10	Throughput versus SNR offset when UE velocity is 5 km/hr	46
3.11	Throughput versus SNR offset when UE velocity is 10 km/hr	47





List of Tables

2.1	Key Deviations in RS Transmission	13
2.2	Path Loss Deviation	16
2.3	List of Key Notations	17
2.4	Simulation Parameters	23
3.1	List of Key Notations	37
3.2	MCS feedback table	42
3.3	Channel Model Related Parameters	42
3.4	Other System Parameters	43

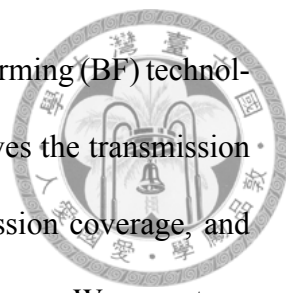


Chapter 1

Introduction

With the ever-increasing number of users and the use of mobile devices, the demand for higher data rates in wireless communication systems is continually increasing. This, in turn, has led the cellular networks for a paradigm shift to address the significantly high capacity requirements. Recently, millimeter-wave (mmWave) frequency bands have been widely recognized as a potential candidate to support emerging broadband-access and cellular system evolution with its achievable coverage comparable to traditional systems [1]-[3]. The mmWave bands, roughly referred to 30 GHz to 300 GHz, has a huge range of available spectrum worldwide. The mmWave transmission is featured with short wavelength, large bandwidth, and sensitive to blockage against most solid materials [4]. Recent study in [1]-[5] shows that, the mmWave channels have the potential to be used in cellular network design, however, much remains to be studied to reach the phenomenal objective. It is also now becoming commercially attractive which has led to many standardization activities. In [6], a detail standardization activity, progress and way forward for short range communication can be found.

The mmWave transmission links are vulnerable and the increased path loss in these



bands are well known. To compensate the increased path loss, beam forming (BF) technology is used to provide high directivity gain [4][5][12], which improves the transmission range. Fig. 1.1 illustrates the effect of frequency bands on transmission coverage, and compensation of the path loss by using narrow beam transmission. In mmWave system, one new dimension added is the BF capability both at the user equipment (UE) and the base station (BS). Due to the use of BF technology and the transmission directivity, finding a reference point for transmission/reception between UE and BS become a very important point of design. In addition, mmWave link availability and reliability is impaired due to its unfavorable propagation characteristics which may have negative implication on network service continuity. It is required to identify and track the best beam pair between a UE and its serving BS which can be used for signaling and data communication. To accomplish this, we present a simple yet novel reference signals (RSs) transmission scheme for mmWave system. RSs are transmitted towards all the UEs served by the BS for beam measurements. This can be used for various purposes e.g. initial access, beam alignment, and channel state information (CSI) measurement.

In the 3GPP LTE system, CRS (cell-specific reference signal) is transmitted by a BS via a sector beam that covers a whole cell . It is delivered in every subframe and all the UEs served by the BS measure the same CRS. In contrast, in mmWave system, we expect a beam-specific reference signal (BRS) may replace the role of the CRS in LTE [10]. It is expected that the BRS is transmitted via a highly directional beam to overcome the significantly larger propagation loss of the mmWave channel. It is note that due to such difference, the studies for microwave frequency based LTE systems are not directly applicable to mmWave system.

Consequently, a RS transmission procedure for mmWave system using highly direc-

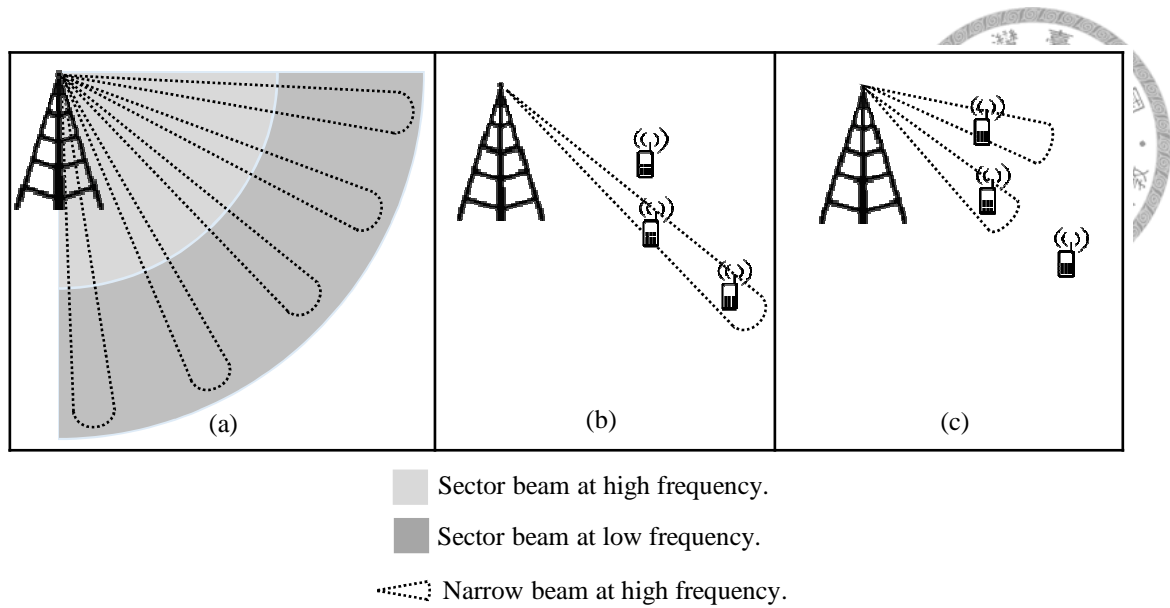


Figure 1.1: (a) Beam coverage at different frequency band using sector and narrow beam, (b) Narrow beam transmitted with full-power, (c) Total transmission power is shared among multiple narrow beams result in smaller coverage.

tional narrow beams where a BS periodically transmits RS beams in different angular directions is needed.

A straightforward solution for RS is to have BSs to transmit directional RS beams in different directions in a sequential manner. Therefore, the RS measurement at UE side is also done in a sequential manner. In this approach, a beam selecting decision can be made after a full measurement on all transmission-reception (TX-RX) beam pairs are performed. For this, a large number of RS transmissions to sweep through the whole angular space is required. The total number of directions for RS transmission in a cell depends on the selected beam-width that is used to cover the desired angular space. Clearly, this approach suffers from higher network overhead and power consumption.

In the aspect of UE, it only concerns itself about specify BS beam which is able to transmit data to it. Therefore, data transmission after waiting all sequential scanning of RS beams is not efficient. A novel scheduling mechanism which is compatible with BRS is also studied in this dissertation.

A slightly refined approach for RS could be to transmit multiple narrow beams to different directions simultaneously to cover the whole desired angular space. However, this, results in lower coverage, and apparently is not beneficial to edge users. Authors in [17], [23] addressed the limitations of this approach with more details.

Chapter 2 of this dissertation presents a hybrid RS pattern design to utilize both single beam and multiple narrow beams transmission. Chapter 3 of the dissertation provides a scheduling mechanism taking BRS sequential scanning into account to not only enhance system throughput but also save UE power. Finally, Chapter 4 concludes the dissertation.



Chapter 2

Directional Reference Signal Design for 5G Millimeter Wave Cellular Systems

2.1 Introduction

A RS transmission pattern design in mmWave cellular system is presented in this chapter. The design provides efficient RS transmission opportunities for reducing channel measurement delay, while ensuring a fair number of RS reception at all UEs within the coverage area. Due to the use of highly directional transmission, a BS might need to sweep through the whole desired angular space to reach all UEs. To ensure RS reception for the cell-edge users, a BS transmits an RS beam in full-power at a time. However, this results in longer time gap between two consecutive RS reception at UE. To overcome this limit, a BS could transmit multiple RS in multiple non-interfering antenna beams in each RS transmission opportunity. The simultaneous RS transmission in multiple beams will be more efficient for providing a specific angular coverage with the trade-off of reduced transmission range as shown in Fig. 1.1(b) and Fig. 1.1(c). In the proposed scheme, we

consider a hybrid design that leverages full-power RS transmission using single beam, and reduced power simultaneous RS transmission using multiple beams to even off the time gap between two consecutive RS reception.



The novelty of our approach lies in the hybrid design that transmits multiple RS beams along with single RS beam. With respect to previous literature, the key contributions we provide in this chapter can be summarized as follows:

- Proposing a hybrid design for efficient RS transmission provisioning in mmWave system.
- Simplifying beam scanning procedure and yet allowing efficiently learning the channel condition.
- Providing a framework for studying the tradeoff between RS transmission overhead and RS measurement accuracy.

The rest of the chapter is organized as follows. We discuss related work in Section 2.2. Section 2.3 gives an overview of the working principles of our proposed scheme. The system model, channel model and mathematical formulations are derived in Section 2.4. The performance evaluation of proposed scheme is presented in Section 2.5. Finally, we conclude this chapter in Section 4 .

2.2 Related Work

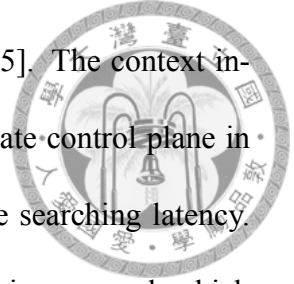
Several works have discussed the CRS design in 3GPP LTE network [7]-[9] under the consideration of a frequency offset between transmitter and receiver. However, the studies for microwave based LTE system are not mmWave compliant due to the less favorable

propagation characteristics of mmWave band. The challenges brought in mmWave system due to the directivity have been studied in, e.g., [11]. The beam tracking procedure and alignment overhead have been widely discussed in [12]-[16]. These studies has primarily investigated on the objective to reduce the beamforming complexity and enhance the searching scope over angular space. The studies in [18]-[20], assumed that the BS beam and UE beam are perfectly aligned. The simplest strategy for beam tracking and alignment is discussed in [13]. It performs an exhaustive search to sweep through all possible directions over the entire angular space by scanning all the BS and UE beam pairs. However, this technique leads to a high beam training overhead and requires longer set-up time. The latency for the initial access might be longer.

In order to alleviate the delayed initial access, authors in [21] proposed a directional cell discovery procedure where the BS periodically transmit synchronization signals in time-varying random directions to scan whole angular space. Findings in this work shows that omnidirectional transmissions of the synchronization signals from the BS generally outperform random directional scanning. However, the omnidirectional transmission of synchronization signals leads to shorter transmission range in control channel, assuming data channel transmission is beamformed [4]. We note that the work in [21] only parallelizes, with our proposed scheme, in the single narrow beam transmission in randomly varying directions but do not uses multiple beam transmission and also do not discuss received power measurement. Authors in [22], [23] compared different initial access design options and evaluated the access delay and system overhead. The analysis in [22] demonstrates significant benefits of low-resolution fully digital architecture in comparison to single stream analog beamforming.

On the other hand, to improve the cell discovery procedure and minimize the delay,

the context-information based procedure has been studied in [23]-[25]. The context information about the UE, e.g., position of UE, is provided by a separate control plane in order to directly steer the beam towards UE for further reducing the searching latency. Recently, in [26], a network assisted small cell discovery mechanism is proposed, which optimizes the UE and network power consumption. However, the discovery delay is not discussed.



2.3 Overview of Proposed Scheme

In this section, we will introduce the concept behind our RS transmission scheme and explain the working procedure of the protocol in detail.

2.3.1 Working Principle

Fig. 2.1 illustrates the overall procedure for proposed hybrid approach for RS transmission (we will call the total transmission period as *Reference Signals Transmission Period (RSTP)* throughout the paper). The model divides the system operation into two stages, namely, (i) Stage-1: Full Reference Signal Transmission Period (**Full-RSTP**), and Stage-2: Efficient Reference Signal Transmission Period (**Efficient-RSTP**). The Efficient-RSTP is further divided into two phases, namely, (i) Scanning Phase (**SP**), and (ii) Compensation Phase (**CP**). In Full-RSTP, BS transmits only one RS beam per time slot using full-transmission power. On the other hand, in Efficient-RSTP, BS transmits multiple RS beams simultaneously per time slot, where the total-transmission power is shared among all the beams. In our design, the Full-RSTP is always followed by one or more Efficient-RSTP, explained later. Remaining in this section, we discuss the overall procedure in detail.

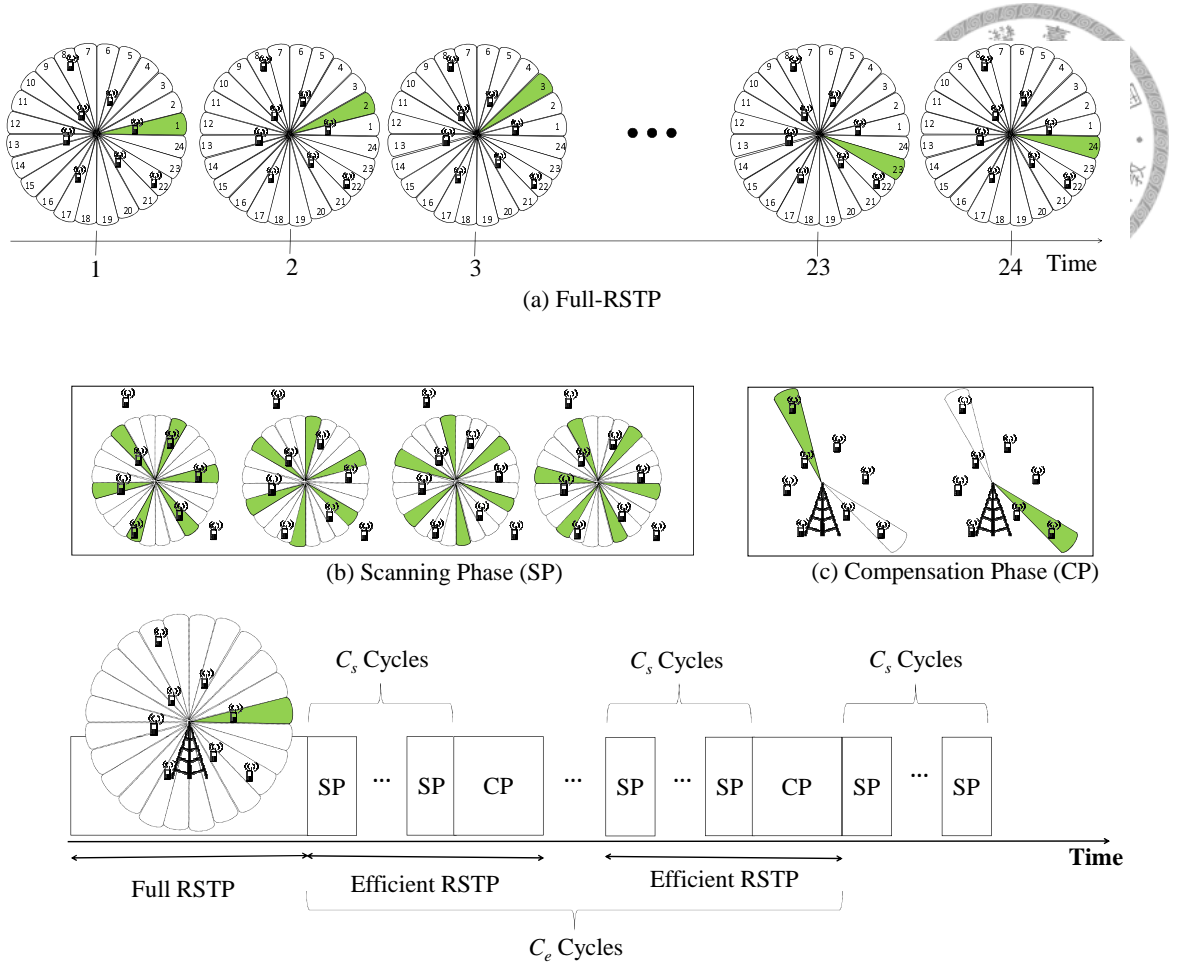


Figure 2.1: Illustration of Proposed Reference Signaling Scheme

2.3.2 Frame Format of Reference Signal

The frame format used by our proposed RS transmission scheme is shown in Fig. 2.2. The frame comprises of \mathcal{T} timeslots. Each time slot is used by BS to transmit RS beam(s). The frame consists of two stages, namely, (i) Stage-1: Full-RSTP, and (ii) Stage-2: Efficient-RSTP. Full-RSTP requires \mathcal{N}_d identical timeslots and is used to transmit a single RS beam per time slot. On the other hand, Efficient-RSTP is further divided into two phases, namely, (i) SP, and (ii) CP. The SP comprises of $\mathcal{N}_d/\mathcal{N}_b$ identical timeslots and is used to transmit \mathcal{N}_b number of RS beam per time slot. The CP consumes ($\leq \mathcal{N}_d$) timeslots, and is used to transmit a single RS beam per time slot on *selected beam*. These beams in CP are selected by BS and will be explained later.

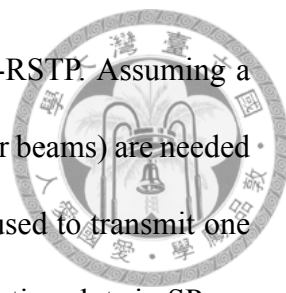


Fig. 2.1(a) illustrates an example of the Stage-1 RSTP, i.e. Full-RSTP. Assuming a beam-width of 15° at BS for transmitting RSs, at most 24 directions (or beams) are needed to cover a 360° angular space. Since each timeslot in Full-RSTP is used to transmit one RS beam, it takes 24 timeslots to cover the whole angular space. The timeslots in SP are used to transmit multiple RS beams simultaneously. As illustrated in Fig. 2.1(b), 6 RS beams are transmitted simultaneously, and it takes 4 timeslots to cover the whole desired angular space. The timeslots in CP are used to transmit RS on selected beams one-by-one as shown in Fig. 2.1(c). This phase uses a variable number of timeslots, i.e. $\leq \mathcal{N}_d$, which depends on the distribution of UE in the cell coverage.

Clearly, over one round of RSTP, there are 1 Full-RSTP, \mathcal{C}_e Efficient-RSTP cycles, and each Efficient-RSTP cycles has \mathcal{C}_s SP cycles and 1 CP cycle, finally, \mathcal{C}_s additional SP cycle towards the end.

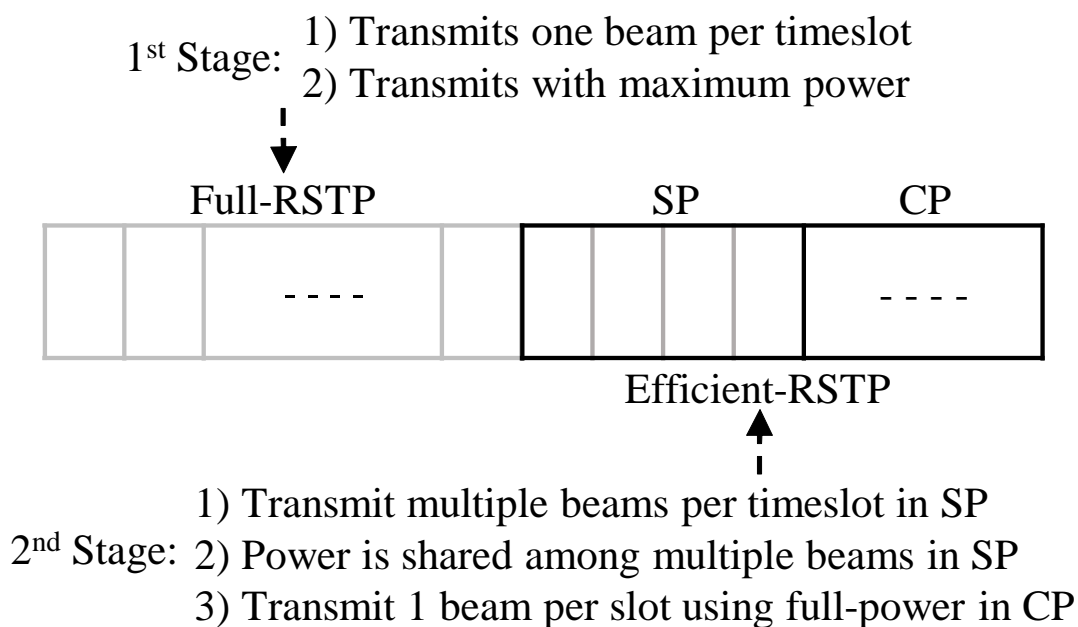


Figure 2.2: Frame format of Reference Signal



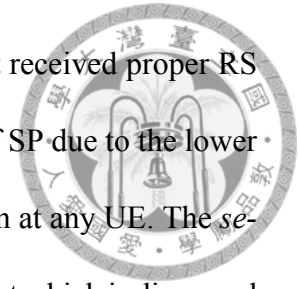
2.3.3 Full Reference Signal Transmission Period

In Stage-1, i.e. in Full-RSTP, BS transmits only one RS beam per time slot with full-transmission power \mathcal{P} . BS sweeps through all \mathcal{N}_d angular directions sequentially to cover the whole angular space. In total, \mathcal{N}_d timeslots are required. The approach proposed in [21] is similar to the Stage-1 procedure here and thus, will be used for performance comparison later. The maximum transmission range of a RS beam transmitted with full-transmission power is designed to be cell radius, d_M . Hence, the RS beams transmitted in this stage can be received by all the users within the cell coverage. These RS beams yield good coverage and specifically is suitable for cell edge users. However, the time gap between two consecutive RS beam received by a particular UE is long. To address this problem, Stage-2 procedure is proposed, i.e. Efficient-RSTP.

2.3.4 Efficient Reference Signal Transmission Period

The Efficient-RSTP always takes place immediately after the Full-RSTP during operation. During the first phase of Efficient-RSTP, i.e. SP, BS simultaneously transmits multiple RS beams per time slot using multiple non-interfering antenna beams. To be specific, \mathcal{N}_b RS beams are transmitted in each time slot. This procedure takes $\mathcal{N}_d/\mathcal{N}_b$ timeslots to sweep through the whole desired angular space, i.e., total \mathcal{N}_d directions. Unlike the Full-RSTP, the total transmission power \mathcal{P} is equally shared among the \mathcal{N}_b multiple RS beams. As a result, the maximum transmission range of a RS beam in Efficient-RSTP is reduced, as illustrated in Fig. 2.4, to D . For UEs positioned beyond this reduced transmission range, D , the RS transmission from BS cannot be properly perceived. To remedy it, the CP phase is thus introduced. In CP phase, the BS transmits RS in some *selected beams* that can cover far UEs, as illustrated in Fig. 2.1(c). It is noted that the beams in CP

phase are selected to provide the coverage for far UEs which cannot receive proper RS transmissions in SP phase. This procedure evens off the limitation of SP due to the lower transmission range as well as increases the frequency of RS reception at any UE. The *selected beams* are identified by the BS from channel measurement report which is discussed in Section 2.3.5. During system operation, one or more consecutive Efficient-RSTP are configured semi-statically over one RSTP.

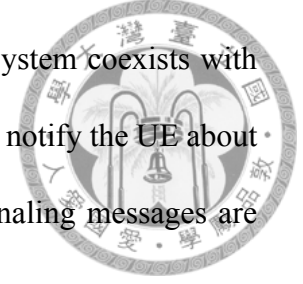


2.3.5 Reference Signal Measurements

So far, only RS transmission is discussed. In the following we explain the design from UE perspective. As discussed, the BS periodically transmits a sequence of RS in non-interfering antenna beams so that UEs can carry out the channel measurement. After receiving RS in Full-RSTP, UEs measure the channel quality of received RS beams and reports it to the BS. With channel quality report from UE, BS decides how many simultaneous beams to be transmitted in SP phases based on certain performance criteria. In addition, BS estimates which UEs may not be able to properly receive RS in SP phase based on the channel quality report. The selected beams which will be used in the CP phase is thus decided. Afterward, BS transmits a *signaling message* to notify the RS beam configuration for the following Efficient-RSTP cycles. The signaling message includes the information about the number of simultaneous beams or transmission power in each beam, as well as selected beams opportunities.

In our system model, RS beams are transmitted in the secondary cell (SCell) which operates in the mmWave band if a mmWave system coexists with LTE, while UE reports channel quality measurement in the primary cell (PCell) operates in the microwave band. However, for a standalone mmWave system UE reports channel quality measurement in

the mmWave band. Similarly, for signaling message, if mmWave system coexists with LTE, the signaling messages are transmitted over microwave band to notify the UE about the RS configuration, while for a standalone mmWave system, signaling messages are transmitted over the mmWave band.

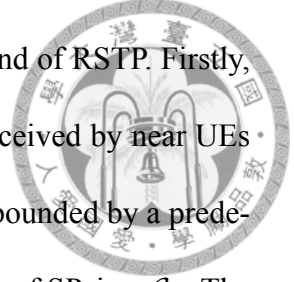


To lay the ground for mathematical analysis on choosing a suitable number of Efficient-RSTP, i.e., C_e , and a suitable number of SP, i.e., C_s , for execution of one RSTP operation in the subsequent section, we summarize the working procedure here. Assuming a UE is reachable during the SP with probability Q_n which depends on the number of simultaneously transmitted beams denoted as \mathcal{N}_b . From the channel quality report of Full-RSTP, BS estimates the received power at each UE when transmission power is reduced to $\mathcal{P}/\mathcal{N}_b$ during SP. If the estimated received power at UE is below \mathcal{P}_m , BS assumes that this UE is not reachable during SP. In this way, the BS estimates the number of UEs that can receive the RS beams during the SP. The probability of UEs which are within the radius D (as shown in Fig. 2.4) to receive the RS beams can thus be estimated from \mathcal{N}_b value. We note that, far UEs or the UEs with worse channel condition only receives RS in CP as well as in Full-RSTP. That said, UEs with bad channel condition only updates their channel condition after the completion of CP. To clearly illustrate how the proposed scheme works over one RSTP period, a comparison in terms of in RS beam transmission type (single/multiple), transmission power in each beam, and transmission range of RS beam for different RS transmission stages, is provided in Table 2.1.

Table 2.1: Key Deviations in RS Transmission

Stages	Tx. Type	No. of RS	Power in Beam	Range
Full-RSTP	Single	1	\mathcal{P}	d_M
SP	Multiple	\mathcal{N}_b	$\mathcal{P}/\mathcal{N}_b$	D
CP	Single	1	\mathcal{P}	d_M

For practical reason, we introduce two constraints when selecting the number of Efficient-



RSTP cycle, C_e , as well as the number of SP cycles, C_s , over one round of RSTP. Firstly, a fairness index which is defined as the ratio of the number of RS received by near UEs to the number of RS received by far UEs is introduced, and is upper bounded by a predefined value η . The fairness constraint has direct effect on the number of SP, i.e., C_s . The second constraint is imposed on the number of timeslots in one round of RSTP, \mathcal{T} and is required to be smaller than a maximum value, \mathcal{T}_{Max} . The constraint affects the number of Efficient-RSTP cycles, i.e., C_e . One of the goal of our proposed scheme is to maximize the number of RS received per time slot at each UE. To address this, BS optimizes the expected number of RS received at UE per slot while meeting above-mentioned constraints. BS chooses an optimal value for N_b to maximize the expected number of RS received at UE per slot. In Fig. 2.3, a detailed working flow is shown.

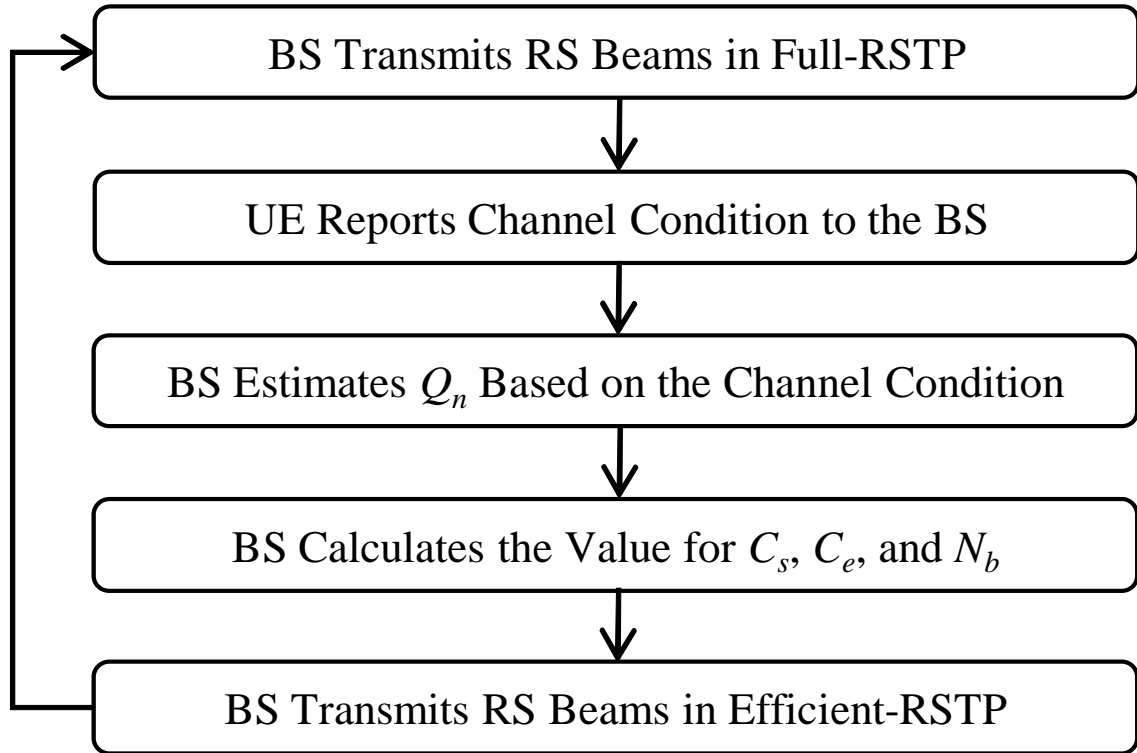
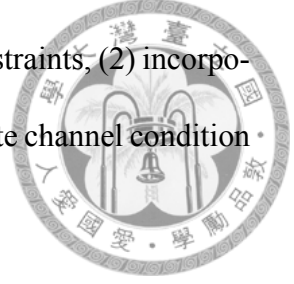


Figure 2.3: Proposed Reference Signaling Flow

To summarize, this scheme is featured with three properties: (1) The expected number



of perceived RS transmissions is increased while meeting the two constraints, (2) incorporating the CP, UEs with worse channel condition, are also able to update channel condition periodically, and (3) the total RS transmission power is constant.

2.4 System Model

2.4.1 Network Model

We consider a mmWave cellular system where transmission and reception are based on high-gain electronically steerable directional antennas. We assume a BS is capable of transmitting either single narrow beam in one direction or multiple narrow beams in multiple directions using non-interfering antenna beams. For analysis, we assume an isolated cell scenario as illustrated in Fig. 2.4. We assumed the UEs are distributed uniformly within the cell coverage with radius d_M . The minimum distance between the BS and UE is denoted as d_m . Furthermore, we assume BS is able to categorize UEs into far UEs and near UEs depending on their respective distance to BS.

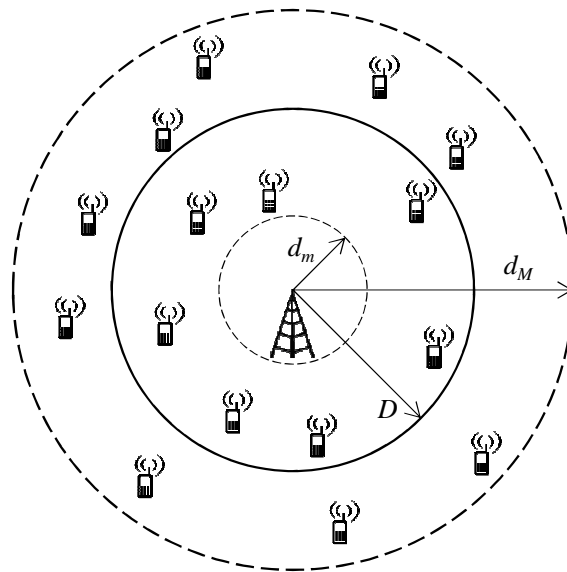


Figure 2.4: The mmWave network model used in this work.

Table 2.2: Path Loss Deviation

carrier frequency	parameter value
28 GHz	$\alpha = 72.0, \beta = 2.92$
38 GHz	$\alpha = 39.1, \beta = 4.0$
73 GHz	$\alpha = 81.9, \beta = 2.7$



2.4.2 Channel Model

Without loss of generality, we consider only Non-Line-of-Sight (NLOS) path loss model. It is noted that an extension to include both NLOS and Line-of-Sight model is straightforward. The NLOS path loss model considered here is expressed by

$$PL(d)[dB] = \alpha + 10\beta \log_{10}(d) \quad (2.1)$$

where d refers to the distance between the BS and UE, $\alpha = 72.0$ and $\beta = 2.92$ are constants from linear regression based on the NLOS measurement provided in [27] for 28GHz. In Table 2.2, a summary of α, β values for different mmWave carrier frequency bands are listed.

Let \mathcal{P}_m denote the minimum required power to correctly decode the RS at the UE side. As discussed in Section 2.3, during the scanning phase, the total transmitting power \mathcal{P} is equally shared among all simultaneously transmitted beams which lead to smaller transmission range, denoted as D . UEs are categorized based on this transmission range. We derive the received power of UE at distance D (as shown in Fig. 2.4) using (2.1) as below.

$$\begin{aligned} \mathcal{P}_m &= \mathcal{P} - PL(d_M) \\ &= \mathcal{P} - 10 \log_{10} \mathcal{N}_b - PL(D) \end{aligned} \quad (2.2)$$

where \mathcal{N}_b is the total number of simultaneously transmitted beams per time slot and d_M refers to the maximum transmission range (distance between the BS and cell boundary).

2.4.3 Mathematical Formulation



In this section, mathematical analysis is performed. Notations used in this chapter are summarized in Table 2.3.

Table 2.3: List of Key Notations

Notation	Description
\mathcal{N}_d	Total number of beam directions in each cell.
\mathcal{N}_b	Number of simultaneously transmitted beam in SP.
\mathcal{P}	Total transmission power [dB] in each cell
d_M	Distance between BS and cell edge.
d_m	Minimum distance between BS and UE.
\mathcal{A}_i	Set of UEs, receives RS from beam i in Full-RSTP.
P_m	Minimum required power to correctly decode the RS.
D	Maximum RS transmitting range in SP.
\mathcal{C}_e	Number of Efficient-RSTP cycles in one round of RSTP.
\mathcal{C}_s	Number of SP cycle in one Efficient-RSTP.
n	Total number of UEs which receives RS.
\mathcal{Q}_n	Probability of UE receiving RS in SP.
\mathcal{U}_n	Set of near UEs which receive RS in SP.
\mathcal{U}_f	Set of far UEs which do not receive RS in SP.
$\mathcal{R}(j)$	The number of RS received by UE j .
\mathbb{U}_t	Expected number of RS received by UE per timeslot.
\mathcal{Q}_f	Prob. of each UEs in \mathcal{A}_i , receives RS in SP by beam i .
\mathcal{T}	Total number of timeslots in one RSTP
\mathcal{T}_{Max}	Maximum number of timeslots in one RSTP
η	The limit or upper bound of fairness index

By (2.2), the reduced RS transmission range D is expressed as

$$D = d_M \mathcal{N}_b^{-\frac{1}{\beta}} \quad (2.3)$$

Since UEs are uniformly distributed within the cell coverage, the probability for a UE receiving RS beam in SP, \mathcal{Q}_n , is proportional to the ratio between the area where near UEs reside and the area where all UEs reside.

$$\mathcal{Q}_n = \frac{\pi D^2 - \pi d_m^2}{\pi d_M^2 - \pi d_m^2} = \frac{\mathcal{N}_b^{-2/\beta} - \left(\frac{d_m}{d_M}\right)^2}{1 - \left(\frac{d_m}{d_M}\right)^2} \quad (2.4)$$



In the second equality of (2.4), we applied (2.3).

Denoting \mathcal{A}_i as the set of UEs which receives RS by the beam i in Full-RSTP. Let E denote the event that $|\mathcal{A}_i| = k$ for the beam i and F denote the event that every UE in \mathcal{A}_i also receives RS by beam i in SP. Essentially, this is a scenario where all UEs, who receives RS by beam i , are near UEs, i.e., positioned within radius D . We can calculate the probability of $|\mathcal{A}_i| = k$ for beam i as,

$$\mathbb{P}\{E\} = \binom{n}{k} \left(\frac{1}{\mathcal{N}_d}\right)^k \left(\frac{\mathcal{N}_d - 1}{\mathcal{N}_d}\right)^{n-k} \quad (2.5)$$

where \mathcal{N}_d is the total number of beam directions and n is the total number of UEs which receives RS in Full-RSTP.

Now, let us assume a scenario where all k number of UEs receive RS in Full-RSTP also receives RS in SP. This means all k number of UEs are positioned within the radius D and its probability expressed as $\mathbb{P}\{F | E\} = (\mathcal{Q}_n)^k$. The probability that every UE in \mathcal{A}_i receives RS in SP by beam i , $\mathcal{Q}_f = \mathbb{P}\{\mathcal{A}_i \subseteq \mathcal{U}_n\}$, is derived as

$$\begin{aligned} \mathcal{Q}_f = \mathbb{P}\{F\} &= \sum_{k=0}^n \mathbb{P}\{F | E\} \mathbb{P}\{E\} \\ &= \sum_{k=0}^n (\mathcal{Q}_n)^k \binom{n}{k} \left(\frac{1}{\mathcal{N}_d}\right)^k \left(\frac{\mathcal{N}_d - 1}{\mathcal{N}_d}\right)^{n-k} \\ &= \left(\frac{\mathcal{Q}_n + \mathcal{N}_d - 1}{\mathcal{N}_d}\right)^n \end{aligned} \quad (2.6)$$

Therefore, the probability of transmitting RS in CP for any beam is $1 - \mathcal{Q}_f$. We calculate the expected number of beam that transmits RS in CP by adding all beams' probability of transmitting RS in CP for a beam, i.e., $\mathcal{N}_d(1 - \mathcal{Q}_f)$.

By definition, the total number of time slot in one round of RSTP, \mathcal{T} , includes the following number of timeslots: (i) \mathcal{N}_d timeslots used for one Full-RSTP, (ii) \mathcal{C}_e Efficient-RSTP with each of Efficient-RSTP comprising \mathcal{C}_s SP and one CP, and (iii) \mathcal{C}_s SP cycles. Thus, the total number of timeslots \mathcal{T} , in one round of RSTP, can be expressed by

$$\begin{aligned}\mathcal{T} &= \mathcal{N}_d + \mathcal{C}_e \left\{ \mathcal{C}_s \left(\frac{\mathcal{N}_d}{\mathcal{N}_b} \right) + \mathcal{N}_d(1 - \mathcal{Q}_f) \right\} + \mathcal{C}_s \left(\frac{\mathcal{N}_d}{\mathcal{N}_b} \right) \\ &= \mathcal{N}_d \left\{ 1 + \mathcal{C}_e \left[\frac{\mathcal{C}_s}{\mathcal{N}_b} + 1 - \mathcal{Q}_f \right] + \frac{\mathcal{C}_s}{\mathcal{N}_b} \right\}\end{aligned}\quad (2.7)$$

Consider \mathcal{R} is a function with its domain $(\mathcal{U}_n \cup \mathcal{U}_f)$, and its image as the number of RS received. Denoting $\mathcal{R}_{\mathcal{U}_f}(i)$ as the number of RS received at each far UE $i \in \mathcal{U}_f$,

$$\mathcal{R}_{\mathcal{U}_f}(i) = 1 + \mathcal{C}_e, \forall i \in \mathcal{U}_f. \quad (2.8)$$

Similarly, the expected number of RS received at each near UE $j \in \mathcal{U}_n$, denoted by $\mathcal{R}_{\mathcal{U}_n}(j)$, is obtained by

$$\mathcal{E}[\mathcal{R}_{\mathcal{U}_n}(j)] = 1 + \mathcal{C}_e[\mathcal{C}_s + 1 - \mathcal{Q}_f] + \mathcal{C}_s, \forall j \in \mathcal{U}_n. \quad (2.9)$$

The expected number of RS received by each UE within the coverage is simply the weighted sum of $\mathcal{R}_{\mathcal{U}_f}(i)$ and $\mathcal{E}[\mathcal{R}_{\mathcal{U}_n}(j)]$. This leads to



$$\begin{aligned}\mathcal{R}_{\mathcal{U}} &= \mathcal{Q}_n \left\{ 1 + \mathcal{C}_e [\mathcal{C}_s + 1 - \mathcal{Q}_f] + \mathcal{C}_s \right\} + (1 - \mathcal{Q}_n)(1 + \mathcal{C}_e) \quad (2.10) \\ &= 1 + \mathcal{C}_s \mathcal{Q}_n + \mathcal{C}_e \left\{ 1 + \mathcal{Q}_n [\mathcal{C}_s - \mathcal{Q}_f] \right\}\end{aligned}$$

where \mathcal{Q}_n and $1 - \mathcal{Q}_n$ is the probability of receiving RS at near UE and far UE, respectively.

Consequently, we derive the expected number of RS received at each UE per time slot as the ratio of expected RS received at each UE in one round of RSTP (2.10) to the total time slot for one round of RSTP (2.7) is, Dividing (2.10) by the total timeslots in one round of RSTP, one obtains the expected number of RS received by UE per timeslot

$$\mathbb{U}_t = \frac{\mathcal{R}_{\mathcal{U}}}{\mathcal{T}} = \frac{1 + \mathcal{C}_s \mathcal{Q}_n + \mathcal{C}_e \left\{ 1 + \mathcal{Q}_n [\mathcal{C}_s - \mathcal{Q}_f] \right\}}{\mathcal{N}_d \left\{ 1 + \mathcal{C}_e \left[\frac{\mathcal{C}_s}{\mathcal{N}_b} + 1 - \mathcal{Q}_f \right] + \frac{\mathcal{C}_s}{\mathcal{N}_b} \right\}}. \quad (2.11)$$

Let η denote fairness constraint which assess the RS received by UE in \mathcal{U}_n to the number of RS received by UE in \mathcal{U}_f . We formulate using (2.8) and (2.9), $\forall i \in \mathcal{U}_n, j \in \mathcal{U}_f$. By definition, the fairness can be obtained by calculating the ratio of (2.9) to (2.8)

$$\begin{aligned}\frac{\mathcal{E}[\mathcal{R}_{\mathcal{U}_n}(j)]}{\mathcal{R}_{\mathcal{U}_f}(i)} &= \frac{1 + \mathcal{C}_e [\mathcal{C}_s + 1 - \mathcal{Q}_f] + \mathcal{C}_s}{1 + \mathcal{C}_e} \\ &= \mathcal{C}_s + \frac{1 + \mathcal{C}_e [1 - \mathcal{Q}_f]}{1 + \mathcal{C}_e} \leq \eta \quad (2.12) \\ &\Rightarrow \mathcal{C}_s \leq \eta - \frac{1 + \mathcal{C}_e [1 - \mathcal{Q}_f]}{1 + \mathcal{C}_e}\end{aligned}$$

Let \mathcal{T}_{Max} be the maximum of \mathcal{T} for one round of RSTP. By (2.7), the constraint on the

total number of timeslots in one RSTP is expressed by

$$\mathcal{N}_d \left\{ 1 + \mathcal{C}_e \left[\frac{\mathcal{C}_s}{\mathcal{N}_b} + 1 - \mathcal{Q}_f \right] + \frac{\mathcal{C}_s}{\mathcal{N}_b} \right\} \leq \mathcal{T}_{Max}. \quad (2.13)$$



Rewriting (2.13), a constraint on \mathcal{C}_e is obtained,

$$\mathcal{C}_e \leq \frac{\frac{\mathcal{T}_{Max}}{\mathcal{N}_d} - 1 - \frac{\mathcal{C}_s}{\mathcal{N}_b}}{\frac{\mathcal{C}_s}{\mathcal{N}_b} + 1 - \mathcal{Q}_f}. \quad (2.14)$$

For simplicity, we consider η as an integer. Therefore, to maximize the expected number of RS received at each UE per time slot, we have the following optimization problem

$$\begin{aligned} & \max_{\mathcal{C}_s, \mathcal{C}_e} \mathbb{U}_t \\ & \text{subject to } \mathcal{C}_s \leq \eta - \frac{1 + \mathcal{C}_e(1 - \mathcal{Q}_f)}{1 + \mathcal{C}_e} \\ & \mathcal{C}_e \leq \frac{\frac{\mathcal{T}_{Max}}{\mathcal{N}_d} - 1 - \frac{\mathcal{C}_s}{\mathcal{N}_b}}{\frac{\mathcal{C}_s}{\mathcal{N}_b} + 1 - \mathcal{Q}_f} \\ & \text{and } \mathcal{C}_s, \mathcal{C}_e, \eta \in \mathbb{Z} \end{aligned} \quad (2.15)$$

where \mathbb{Z} denotes the set of all integers. We then relax \mathcal{C}_e as a real variable to derive closed form solution for following optimization problem.



$$\begin{aligned}
& \max_{\mathcal{C}_s, \mathcal{C}_e} \mathbb{U}_t \\
& \text{subject to } \mathcal{C}_s \leq \eta - \frac{1 + \mathcal{C}_e(1 - \mathcal{Q}_f)}{1 + \mathcal{C}_e} \\
& \mathcal{C}_e \leq \frac{\frac{\mathcal{T}_{Max}}{\mathcal{N}_d} - 1 - \frac{\mathcal{C}_s}{\mathcal{N}_b}}{\frac{\mathcal{C}_s}{\mathcal{N}_b} + 1 - \mathcal{Q}_f} \\
& \text{and } \mathcal{C}_s, \eta \in \mathbb{Z}
\end{aligned} \tag{2.16}$$

By examining (2.12), one can see that $\eta - 1 \leq \eta - \frac{1 + \mathcal{C}_e[1 - \mathcal{Q}_f]}{1 + \mathcal{C}_e} \leq \eta - \frac{1}{1 + \mathcal{C}_e}$. Therefore, maximal \mathcal{C}_s is in $[\eta - 1, \eta - \frac{1}{1 + \mathcal{C}_e}]$. Suppose η is an integer, substitute $\eta - 1$ for \mathcal{C}_s in (2.14). When equality holds in (2.14), we derive the optimal value for \mathbb{U}_t from (2.11) as,

$$\mathbb{U}_t^* = \frac{\mathcal{N}_b \left\{ [\mathcal{Q}_n(\eta - 1) + 1] \left[\frac{\mathcal{T}_{Max}}{\mathcal{N}_d} - \mathcal{Q}_f \right] - \mathcal{Q}_n \mathcal{Q}_f \left(\frac{\mathcal{T}_{Max}}{\mathcal{N}_d} - \frac{\eta - 1}{\mathcal{N}_b} - 1 \right) \right\}}{\mathcal{T}_{Max} [\eta + \mathcal{N}_b(1 - \mathcal{Q}_f) - 1]} \tag{2.17}$$

where \mathbb{U}_t^* is the optimal value of \mathbb{U}_t .

2.5 Performance Evaluation and Analysis

In this section, we evaluate the performance of our proposed RS transmission scheme and provide the key findings.

To analyze the performance of our RS transmission scheme, we compare it with two other schemes: *Without-Efficient-RSTP*, and *Without-Compensation Phase*. The *Without-Efficient-RSTP* is the simplest directional scanning method proposed in [21]. It is noted that our proposed scheme degrades to the approach proposed in [21] when ignoring the Stage-2, i.e., *Efficient-RSTP*.

We study the performance of our scheme against two metrics: *average number of RS received at each UE*, and *expected number of RS received at each UE*. The basic system parameters used for simulation and theoretical analysis are listed in Table 2.4. The related parameters are based on [27],[29]. The evaluation scenario follows the description of Section 2.4.1 and Section 2.4.2.

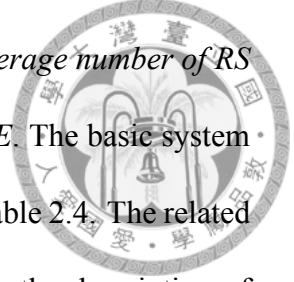
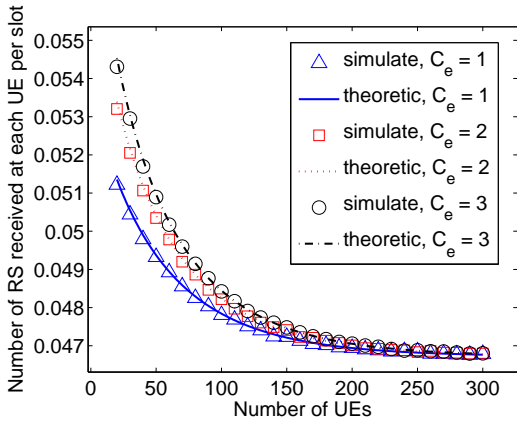


Table 2.4: Simulation Parameters

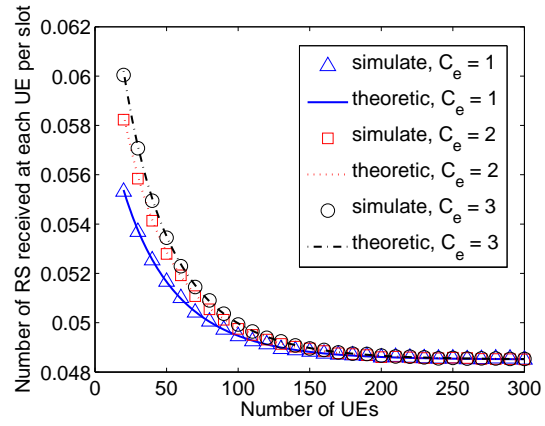
Item	Value
Thermal noise level	$-174 \text{ dBm}/\text{Hz}$
Downlink bandwidth	100 MHz
BS transmit power	37 dBm
BS antenna gain	10 dBi
Carrier frequency	28 GHz
Path loss parameter, $PL = \alpha + 10\beta \log_{10}(d)[\text{dB}]$, d in meters	$\alpha = 72.0, \beta = 2.92$
Minimum SNR to correctly decode the RS	-10 dB
UE receiver noise figure	10 dB
Minimum distance between BS and UE	10 m
Beamwidth	15°

Fig. 2.5 demonstrates the simulation result and theoretic result for average number of RS received and expected number of RS received at each UE per time slot, respectively, versus the number of UE on varying the number of Efficient-RSTP cycles. The theoretic result is defined as the ratio of the expected number of RS received at each UE to the total number of timeslots \mathcal{T} in one round of RSTP. Interestingly, the theoretical observations using (2.11) and experiment results are uniform. Therefore, the simulation result validates the mathematical formulations. We observed that regardless the number of Efficient-RSTP cycles (C_e), the proposed scheme converges the expected RS received at each UE per time slot in about 250 UEs. To perform this experiment, we have fixed $C_s = 2$ for all value of C_e and executed simulation on different \mathcal{N}_b values.

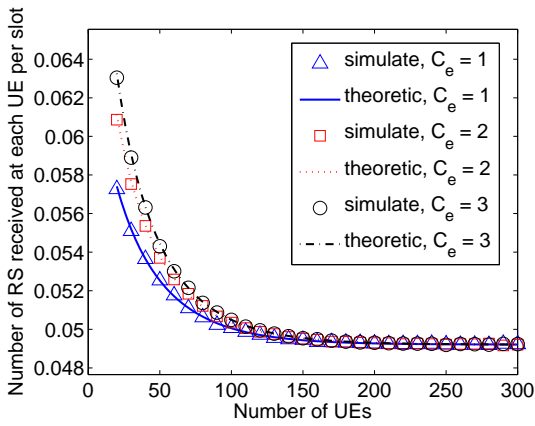
Observation 1. *The expected number of RS received at each UE per time slot decreases with increasing number of UE and finally converges, even on different C_e values.*



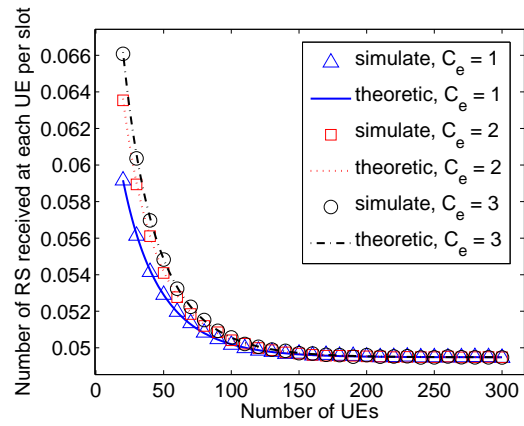
(a) For $\mathcal{N}_b = 2, \mathcal{C}_s = 2$



(b) For $\mathcal{N}_b = 3, \mathcal{C}_s = 2$



(c) For $\mathcal{N}_b = 4, \mathcal{C}_s = 2$



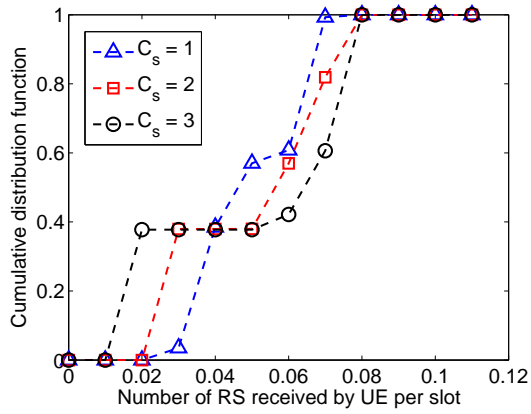
(d) For $\mathcal{N}_b = 6, \mathcal{C}_s = 2$

Figure 2.5: The number of RS received at each UE per time slot varying Efficient-RSTP cycles and $\mathcal{N}_b = \{2, 3, 4, 6\}$.

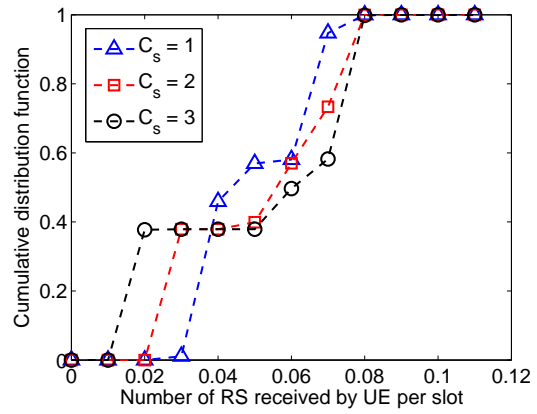
From (2.6), we observed that Q_f decreases exponentially with the increase in the number of UEs. Therefore, it is advisable to incorporate CP while the number of UEs are higher. All curves converge because of the probability, regardless of the C_e value. The proposed scheme finally converges to a Full-RSTP followed by C_s SP. Considering that n tends to infinity will result in Q_f tending to 0, (2.11) tends to $\frac{1+C_s Q_n}{\mathcal{N}_d(1+C_s/\mathcal{N}_b)}$, which equals the expected RS received at each UE per time slot under a simpler scheme which is a Full-RSTP followed by C_s number of SP.

Observation 2. Increasing C_s results in more frequent RS reception at near UE per time slot comparing to which of far UE.

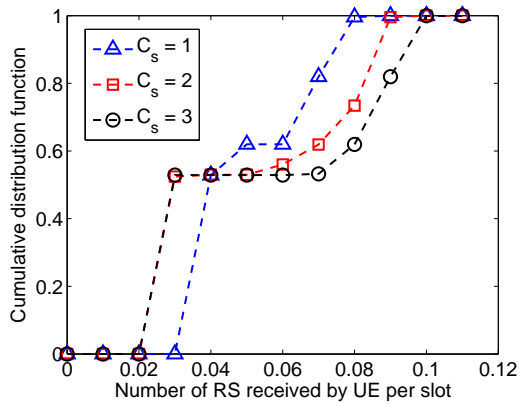
We execute simulation on different number of \mathcal{N}_b and C_e , and plot the results in Fig.



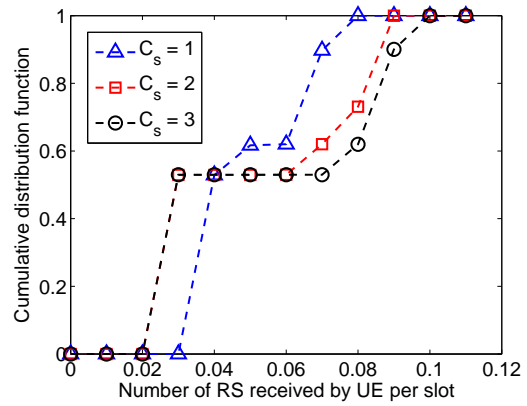
(a) For $\mathcal{N}_b = 2, \mathcal{C}_e = 2, n = 75$



(b) For $\mathcal{N}_b = 2, \mathcal{C}_e = 4, n = 75$



(c) For $\mathcal{N}_b = 3, \mathcal{C}_e = 4, n = 75$



(d) For $\mathcal{N}_b = 3, \mathcal{C}_e = 2, n = 75$

Figure 2.6: The cumulative distribution function (CDF) of RS received per time slot for different SP cycles.

2.6. We have performed this experiment with 75 UEs in the cell. The number of UE decided for the experiment is according to [30] settings¹. From Fig. 2.6 which plots cumulative distribution function (CDF) for the number of RS received per time slot, we observe that as \mathcal{C}_s increase, both lower RS received per time slot portion of UE and higher RS received per time slot portion of UE increases. It concludes that the fairness in system is deteriorated as \mathcal{C}_s increases. UE in \mathcal{U}_n is able to receive RS whereas the UE in \mathcal{U}_f is not able to receive RS during SP. Near UE receives RS in SP as well as in CP which in turn receives more frequent RS. Therefore, the number of RS received by UE in \mathcal{U}_n increases on increasing \mathcal{C}_s . On the other hand, UE in \mathcal{U}_f needs to wait longer duration to receive

¹According to the 3GPP Evolved Universal Terrestrial Radio Access (E-UTRA), UE density across a cell is set to 25 when UEs are distributed uniformly.

RS. As a result, the frequency of receiving RS for far UEs is less or not frequent.

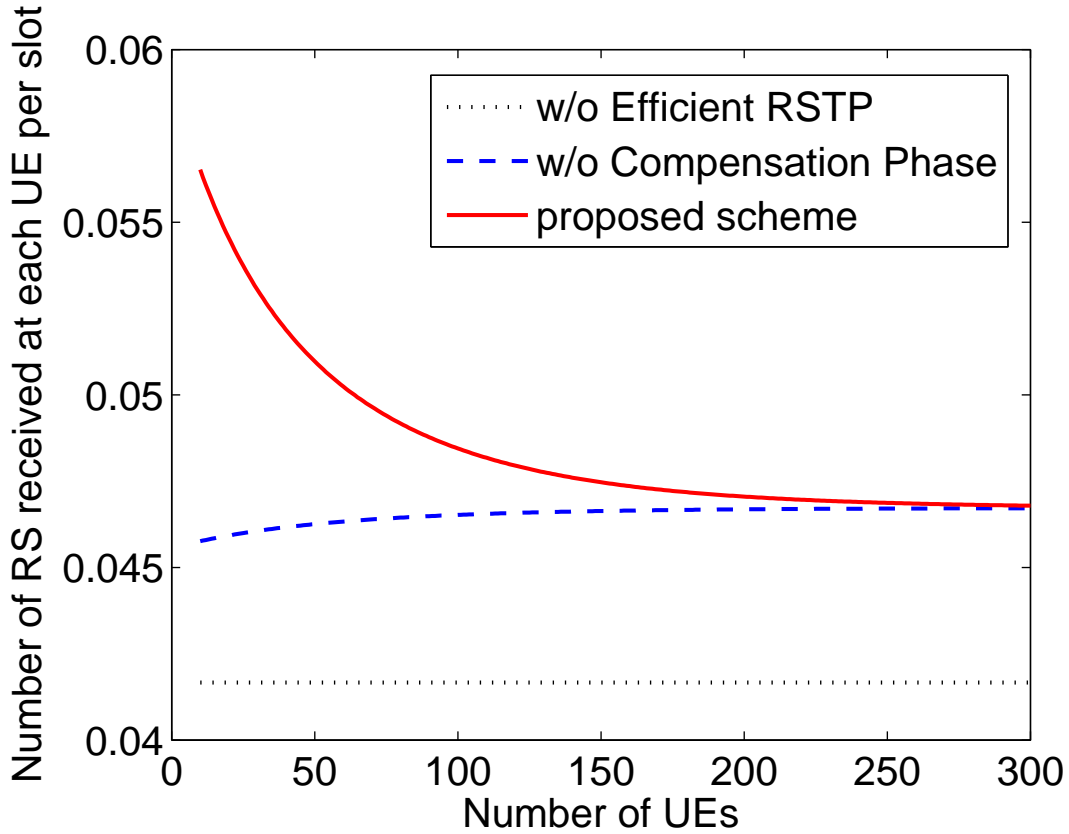


Figure 2.7: Performance comparison of three different schemes. $\mathcal{N}_b = 2$, $\mathcal{C}_s = 2$ and $\mathcal{C}_e = 3$.

Observation 3. *The proposed RS transmission scheme outperforms other two schemes.*

In Fig. 2.7, we plot theoretic result by (2.11) for the proposed scheme. We assume that the proposed scheme and *w/o Compensation Phase* is compared under the same fairness constraint. We denote the number of cycles of SP in *w/o Compensation Phase* is as \mathcal{C}'_s .

From (2.12), we derive \mathcal{C}'_s as below.



$$\begin{aligned} \mathcal{C}_s + \frac{1 + \mathcal{C}_e[1 - \mathcal{Q}_f]}{1 + \mathcal{C}_e} &= \frac{1 + \mathcal{C}'_s}{1} \\ \Rightarrow \mathcal{C}'_s &= \mathcal{C}_s - \frac{\mathcal{C}_e \mathcal{Q}_f}{1 + \mathcal{C}_e} \end{aligned} \quad (2.18)$$

The expected RS received at each UE per time slot for *w/o Compensation Phase* is

$$\frac{\mathcal{Q}_n(1 + \mathcal{C}'_s) + (1 - \mathcal{Q}_n)}{\mathcal{N}_d + \mathcal{C}'_s \frac{\mathcal{N}_d}{\mathcal{N}_b}} = \frac{1 + \mathcal{Q}_n \mathcal{C}'_s}{\mathcal{N}_d(1 + \frac{\mathcal{C}'_s}{\mathcal{N}_b})} \quad (2.19)$$

Fig. 2.7 compares the performance of three different schemes. Given a fixed \mathcal{N}_b (we have set $\mathcal{N}_b = 2$ for this test), we studied the expected RS received at each UE per time slot. A simpler scheme *w/o Compensation Phase* is compared with the proposed scheme under the same fairness constraint. The *w/o Efficient-RSTP* scheme is discussed in [21]. As shown in the theoretic result plotted by (2.11) and (2.19), the proposed scheme without a compensation phase results in smaller expected number of RS received at each UE per time slot. To counterbalance the less amount of RS received at far UE, *w/o Compensation Phase* scheme needs to frequently use the Full-RSTP. On the contrary the same can be easily achieved using CP instead Full-RSTP again. Thus, the proposed scheme without an CP is less efficient than our proposed scheme. The other two schemes outperform *w/o Efficient-RSTP* of which the expected number of RS received at each UE per time slot is $\frac{1}{\mathcal{N}_d}$. Another important observation we found is that, these two scheme converges on higher UE presence because the proposed scheme converges to a Full-RSTP followed by \mathcal{C}_s number of SP without using a CP as mentioned-previously in Observation 1.

Fig. 2.8 shows both the average number of RS received and the expected number of

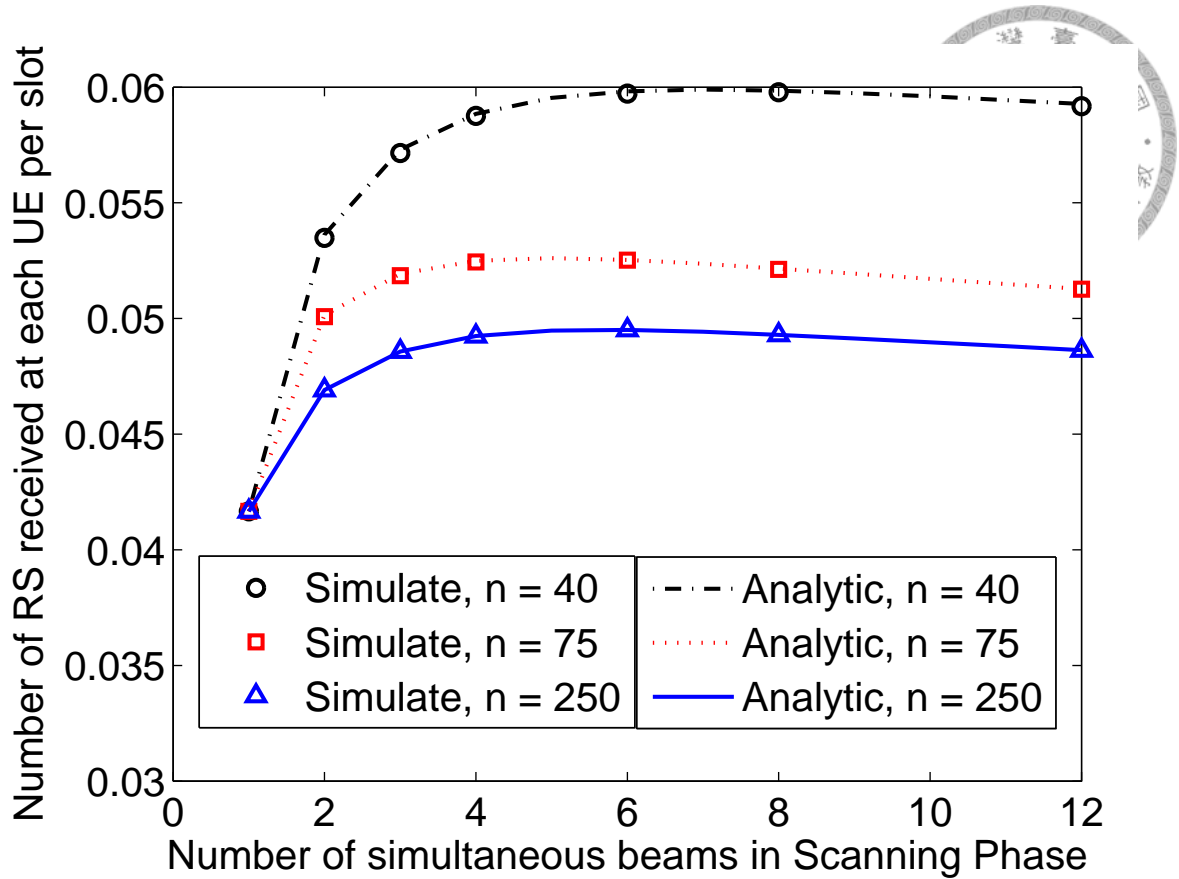
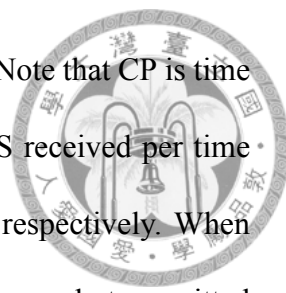


Figure 2.8: The number of RS received per time slot for different number of simultaneous beam in SP varying number of UEs. Here, we set $\eta = 3$ and $\mathcal{T}_{Max} = 600$.

RS received at each UE per time slot varying \mathcal{N}_b . We calculate the expected number of RS received at each UE per time slot using (2.16) for a real value of \mathcal{C}_e . On the other hand, we execute simulation for multiple times to find the average number of RS received for a discrete value of \mathcal{C}_e . For this experiment, we set $\mathcal{C}_s = \eta - 1$ and in analytic result \mathcal{C}_e is set to the boundary value of (2.14), which is the feasible solution. In simulation result, \mathcal{C}_e is rounded to the nearest integer less than or equal to the value of \mathcal{C}_e which is set in analytic result. On $\mathcal{N}_b = 1$, the proposed protocol degrades to Full-RSTP. We found, the expected RS received at each UE per time slot is concave. Interestingly, from simulation results, we observe that, increasing the number of simultaneously transmitted beams in SP does not definitely lead to larger average number of RS received at each UE per time slot. Since, the number of simultaneously transmitted beams in SP is inversely proportional to



the transmission range in SP which leads to more possible to use CP. Note that CP is time consuming because of single beam transmission. The number of RS received per time slot is optimal at $\mathcal{N}_b = 8, 6, 6$ for the number of UE $n = 40, 75, 250$, respectively. When the number of UE is smaller, BS prefer using more number of simultaneously transmitted beams in SP because less probability using CP in small number of UE from (2.6). We conclude that \mathcal{N}_b can be chosen depending on the number of UEs in the coverage. We can get the optimized \mathcal{N}_b by integer linear search among all \mathcal{N}_b using (2.17) or any other integer optimization method. Another observation we have from this result is that the average number of RS received per time slot in simulation result is less than or equal to analytic result because \mathcal{C}_e in simulation result is less than or equal to the value of \mathcal{C}_e in analytic result.

In Fig. 2.9, we perform the analytic experiment on different mmWave bands to study the expected number of RS received at each UE per time slot with varying \mathcal{N}_b in SP phase. The proposed scheme yields higher number of RS reception at each UE per slot over single beam transmission, which is the baseline. The performance differentiation in different mmWave bands are due to the path loss characteristics which lead to different optimal \mathcal{N}_b for different bands. In short, the number of simultaneous beam transmission and UE distribution in cell can have a great impact on the RS transmission and for fair RS reception at UE.

2.6 Summary

This chapter proposes a new scheme to transmit reference signal so as to boost rate of receiving reference signal at each UE. We have studied the problem of reference signals design that are used by BS to learn the channel condition. A hybrid design is proposed

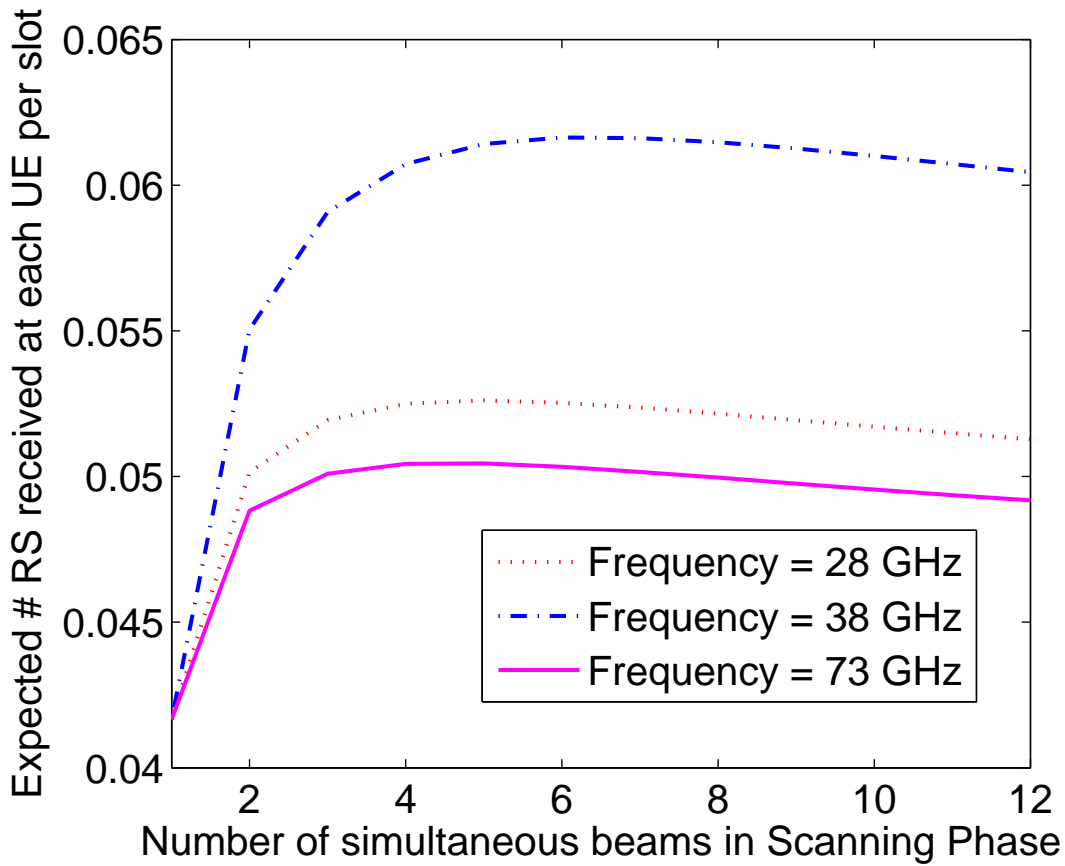
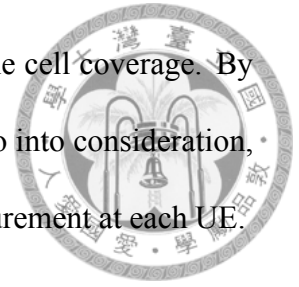


Figure 2.9: Performance variation due to different mmWave carrier frequencies when number of UE $n = 75$, $\eta = 3$, and $\mathcal{T}_{Max} = 600$.

for efficient reference signal transmission provisioning in mmWave cellular system. By considering fairness and periodicity of transmission pattern, we study the problem of maximizing reference signal reception at each UE per time slot and formulate an optimization problem. We then establish a simple protocol to help BS to find an optimal solution. In this scheme, BS periodically configures reference signal transmission pattern according to UE reporting channel information. Our proposed scheme simplify the beam scanning procedure while providing efficient reference signal transmission reducing the channel measurement delay. The performance of this scheme is evaluated by simulation and compared with mathematical formulation. Simulation results not only validate our mathematical formulation but also demonstrate that our scheme outperforms others. The simulta-

neous multiple beam transmission especially suits for near UEs in the cell coverage. By explicitly taking small number of UE in mmWave small-cell scenario into consideration, our scheme provides a desirable solution to frequently channel measurement at each UE.





Chapter 3

Scheduling Mechanism for 5G

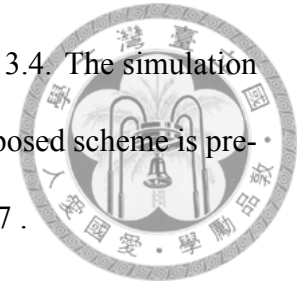
Millimeter Wave Cellular Systems

3.1 Introduction

This chapter provides a scheduling mechanism for 5G mmWave cellular systems. Reference signal (RS) which is transmitted beam by beam leads to time difference in channel measurement. This time difference in channel measurement can cause transmission fail due to outdated channel information. In traditional cellular network, RS is transmitted to cover whole sector. Therefore, it would seem that further investigations are needed to study the scheduling mechanism in mmWave cellular systems. In this study, a channel measure delay aware scheduling mechanism on directional reference signaling is proposed to enhance throughput and save UE power. An expression of system throughput is derived from Markov chain modeling in order to provide insight under different setting of system.

The rest of the chapter is organized as follows. We discuss related work in Section 3.2. Section 3.3 introduces an scenario which we study. The working principles of our pro-

posed scheme and mathematical formulations are derived in Section 3.4. The simulation detail is provided in Section 3.5. The performance evaluation of proposed scheme is presented in Section 3.6. Finally, we conclude this chapter in Section 3.7 .



3.2 Related Work

Several research is studied on utilizing adaptive modulation and coding scheme (MCS) selection to improve throughput or spectrum efficiency. Fan [31] discusses resource block assignment and MCS selection to improve throughput since the same MCS must be selected to every resource block for single user in one transmission time interval (TTI). The time between channel quality indicator (CQI) estimation and scheduling can cause improper MCS. The event is called CQI aging. CQI aging can degrade throughput or spectrum efficiency [32]. In this incident, reinforcement learning technique can be applied to improve CQI accuracy [33]. CQI aging is described as outdated CQI and its impact on throughput is derived from assuming Jakes model in [34]. However, directional antenna for mmWave scenario is not compliant with Jakes model. Instead, the method of using finite-state Markov chain to model fading channel is well developed [35]. Viswanathan [36] models Rayleigh fading channel as finite-state Markov channel to study capacity which is affected by CSI feedback delay. Chen [37] introduces a first-order finite state Markov model to study channel fading effect between CQI feedback and HARQ retransmissions.

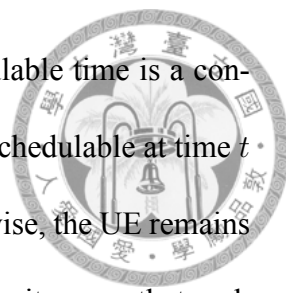
3.3 System Model



A system where a BS operating at 28 GHz placed in the center is considered to serve UEs around it. The contour of BS coverage is a circle which centers at BS. UEs are placed uniformly within BS coverage except the region inside the shortest legal distance which is 10 m between UEs and BS. The BS is equipped with directional antennas which utilize code-book based beamforming. The BS is composed of three sectors and each sector is able to beamform eight directional beams. We assume that BS knows each best beam pair, which is able to achieve largest power transmission, to serve UEs in the beginning. Serving beam pairs do not change during reference signaling and data transmission. We assume our traffic model is only downlink and full buffer. We assume that both transmission time interval (TTI) and CQI feedback delay is 0.5 ms. We assume CQI measurement by UE is perfect without error. We assume transmission throughput becomes 0 when actual channel required CQI is below which used to transmit. A slot comprises a negligible overhead of RS and a TTI. When BS simultaneously transmits data to multiple UEs in the same TTI, the throughput in single UE is divided by total number of UEs simultaneously served. There is no interference between UEs when they are simultaneously served by BS. We assume that UE movement trajectory is a line. When a UE moves between two end points, its channel response is interpolated from which of two end points.

3.4 Proposed Scheduling Mechanism

In our proposed scheduling mechanism, the UE transits to high power state for receiving RS and starts its schedulable time after receiving RS. UE feedbacks CQI after the UE receiving RS from BS and BS receives CQI from the UE after a slot duration delay. The



schedulable time of UE is triggered right after receiving RS. Schedulable time is a continuous time period when the UE is schedulable. A UE is said to be schedulable at time t when a BS can schedule for data transmission to UE at time t . Otherwise, the UE remains in the low power state to save power. When schedulable time is T slots, it means that each UE becomes schedulable T slots after receiving RS from BS. UEs utilize this mechanism to not only save power when no data transmission but also reduce delay time between CQI report and data transmission. The mechanism is illustrated in Fig. 3.1.

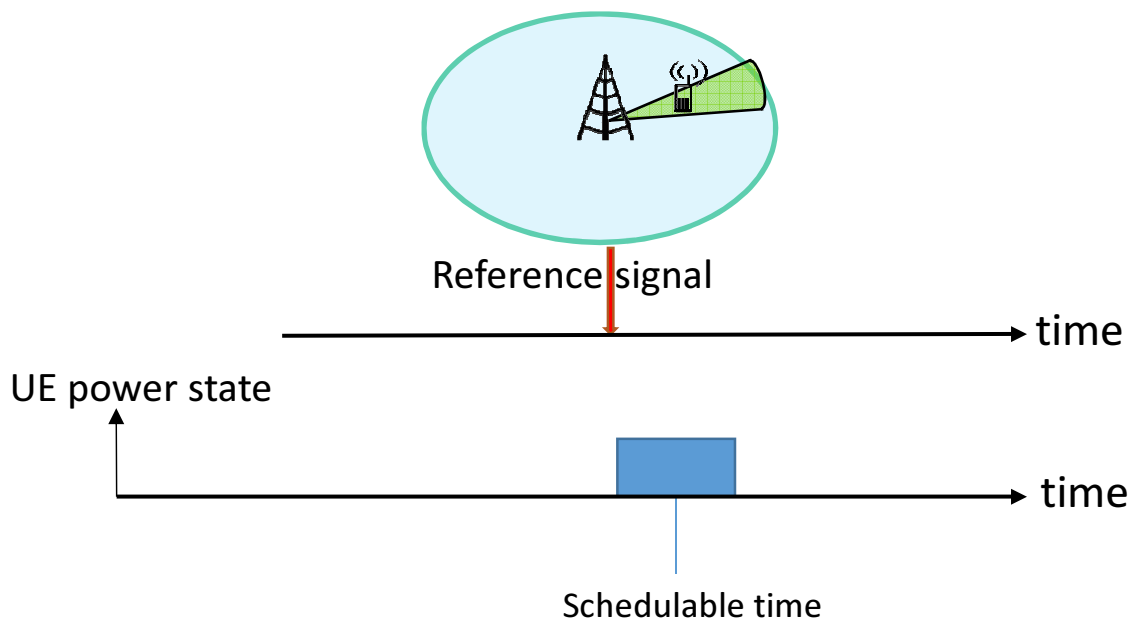
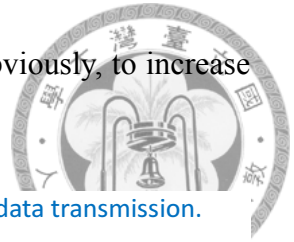


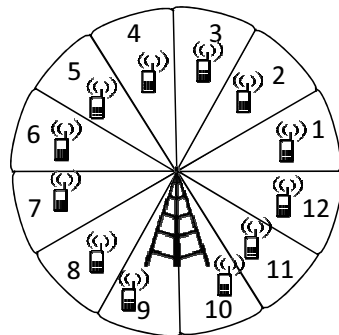
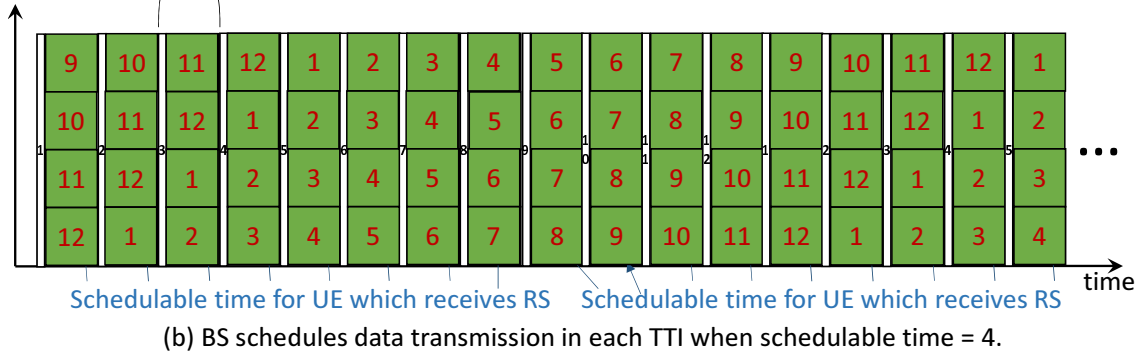
Figure 3.1: illustration for UE power state transition right after reference signal

Schedulable device set is the set of UEs that are schedulable at a given time t . A BS schedules data transmission for all UEs within the schedulable device set in each TTI. Fig. 3.2 illustrates an example of BS scheduling data transmission in each slot. In this example, we assume that $T = 4$ and BS transmits single RS beam in each slot to sequentially sweep all beams. Therefore, BS must schedule UEs which receive any RS in previous four slots. That is, the UE which associates with any four beams that transmit RS in previous four slots will be scheduled for data transmission. In this example, schedulable

device set include the UEs which associate with any four beams. Obviously, to increase the schedulable time will increase the size of schedulable device set.



A time slot is composed of a reference signal transmission and data transmission.



- n Beam n reference signal
- m Schedulable time for UE which receives beam m reference signal

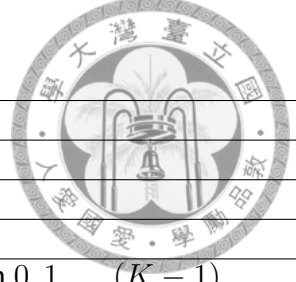
(a) BS transmit a RS beam in a slot and sequentially sweep all beam in 12 slots.

Figure 3.2: An example of scheduling data transmission for schedulable time = 4 slots

We consider a first order finite state Markov chain to model channel CQI transition of UE. Let t be the t th slot for the UE after receiving RS, K be the number of MCS which can be selected. CQI index from $0, 1, \dots, (K - 1)$. Let P be the CQI state transition probability matrix which is a $K \times K$ matrix, C_i be the BS transmission rate for CQI i , r be the initial probability distribution of CQI in channel, R_i be the average throughput over schedulable time when CQI i is measured and feedback, ρ be the average distribution of CQI measured to transmit data, \mathcal{N}_d be the total number of beam directions in a site. Notations used in this chapter are summarized in Table 3.1.

By eliminating the transmission rate in transition to lower CQI than reported CQI and averaging throughput over schedulable time T slots, we then derive R_i as

Table 3.1: List of Key Notations



Notation	Description
\mathcal{N}_d	Total number of beam directions in each site
T	Number of slots in schedulable time
t	The t th slot for the UE after receiving RS
K	Number of MCS which can be selected. CQI index from 0, 1, ..., $(K - 1)$
P	CQI state transition probability matrix P which is a $K \times K$ matrix
C_i	BS transmission rate for CQI i
r	The initial probability distribution of CQI in channel
R	R is a $K \times 1$ matrix. R_i which is the entry of the i th row of R denotes the expected throughput over schedulable time when CQI i is measured and feedback.
δ_t	Probability distribution of CQI after t th slot
ρ_t	Normalized distribution of CQI after t th slot
η	System throughput in one slot

$$R_i = \frac{C_i}{T} \sum_{t=1}^T \sum_{j=i}^{K-1} P_{ij}^t \quad (3.1)$$

From characteristics of Markov chain, we derive δ_t , distribution of CQI after t th slot, as

$$\delta_t = rP^t \quad (3.2)$$

BS does not allocate resource block to UEs which report CQI 0. Therefore, we only need to consider CQI distribution on CQI 1 to $K - 1$. By normalizing (3.2), we derive ρ_t , normalized distribution of CQI after t th slot, as

$$\rho_t = \frac{\delta_t}{\sum_{i=1}^{K-1} (\delta_t)_i} \quad (3.3)$$

Finally, we take the average of \mathcal{N}_d slots to derive system throughput in one slot, η as

$$\eta = \frac{\sum_{t=0}^{\mathcal{N}_d-1} \rho_t}{\mathcal{N}_d} R \quad (3.4)$$

3.5 Simulator



We extend the simulator from [38], which is modified from the 3GPP spatial channel model(SCM) [39]. We further expand number of BS and UE antenna element. We utilize explicitly positioned scatters which are generated from the delay of the paths, angle of arrival (AoA) and angle of departure (AoD). We calculate cluster power fraction by linear interpolation to support continuous channel behavior of UE mobility according to [40]. According to the 3GPP SCM [39], BS antenna pattern used for each sector is defined by

$$A(\theta) = -\min\left[12\left(\frac{\theta}{\theta_{3dB}}\right)^2, A_m\right] \quad (3.5)$$

where θ_{3dB} is the half power beam width (HPBW) of antenna in degrees and A_m is maximum attenuation in dB which is the antenna gain far away from the antenna bore sight. We set $\theta_{3dB} = 65^\circ$ and $A_m = 30$ dB in our directional antenna simulation. BS antenna gain pattern is plotted in Fig. 3.3.

A BS comprise three sector of directional antenna. Each sector serve 120° degrees of area span. There are 8×4 antenna element in each sector of our directional antenna. The directional antenna use code-book based beamforming technology which can select from eight antenna weight for each antenna element to form eight directional beams. The magnitude of eight directional beams of antenna field pattern is plotted in Fig. 3.4.

The different magnitude in each BS directional beam results from different BS antenna gain pattern at each azimuth in degrees.

UE antenna Gain pattern is omnidirectional. There are 4×4 antenna elements in UE. It use code-book based beamforming technology which can select from four antenna weights for each antenna element to form four directional beams. The beam patterns of

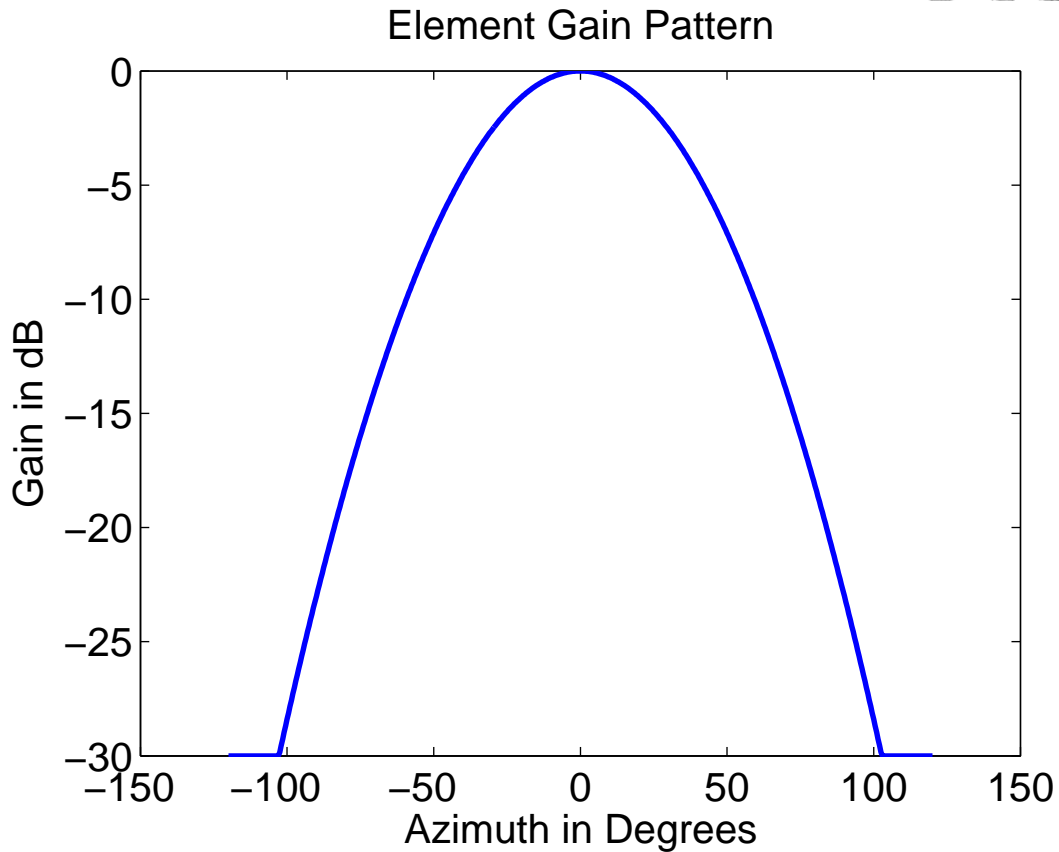


Figure 3.3: BS antenna Gain pattern

UE is shown in Fig. 3.5.

UEs measure CQI based on receiving SNR. We utilize the mapping table for CQI to SNR threshold with 10% block error rate (BLER) shown in Table 3.2 from [31]. UE reports the highest CQI whose corresponding SNR threshold with 10% BLER is below the UE receiving SNR.

Our channel model related parameters and other system parameters are summarized in Table 3.3 and Table 3.4, respectively. Most of settings of parameter are from [38] and [40]. Parameters which are not mentioned in these table are the same as in **Chapter 2** simulation setting. We utilize Shannon's channel capacity equation to calculate throughput.

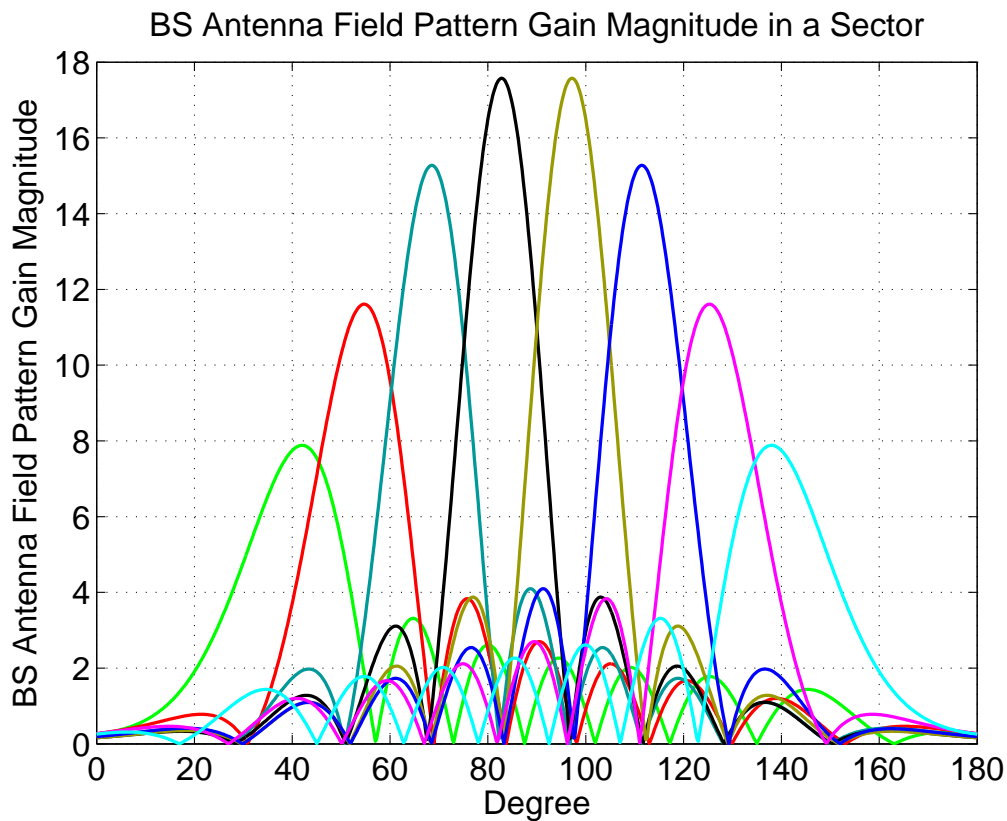


Figure 3.4: BS antenna field pattern gain magnitude at each directional beam

3.6 Evaluation and Results

In this section, we evaluate the throughput under different setting of schedulable time, UE velocity and SNR offset in choosing CQI.

The simulation results of simulator is shown in Fig 3.6, where UEs velocity is fixed as 5 km/hr. Fig 3.6 (a), (b), (c) demonstrate the throughput component in each successive step of slot after receiving RS. The sum of throughput in each slot is system throughput which is plots in Fig 3.6 (d). The transition probability is able to be extracted from simulator. We take average of thirty-thousand UE of simulation to extract the transition probability. We use Markov chain model to simulate system throughput and compare with the calculation at (3.4) in Fig. 3.7. The simulated results by realistic channel model are also provided. The theoretic results from calculation of Markov model are very close to the simulated

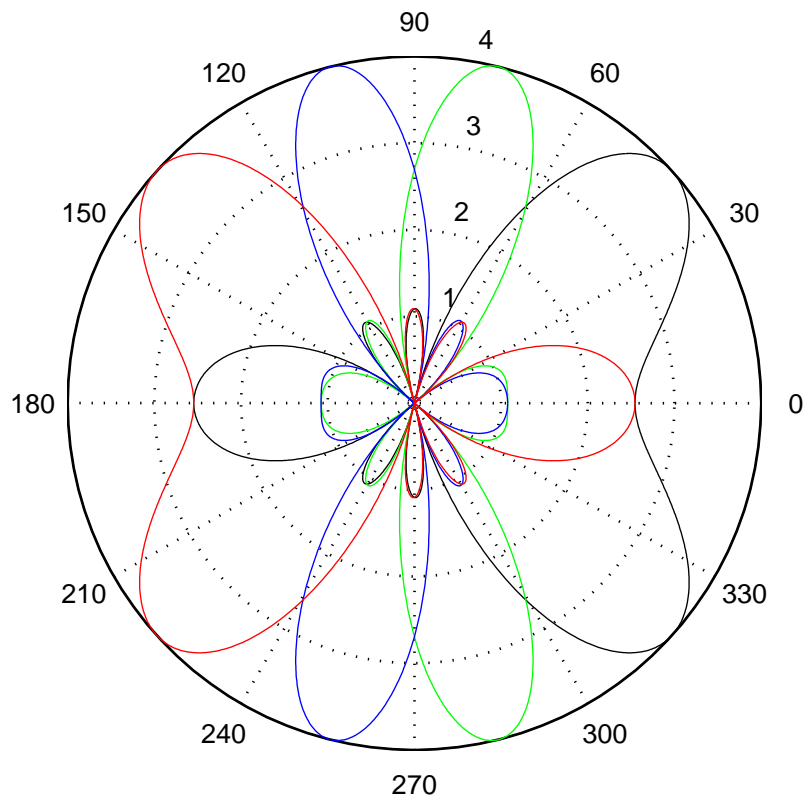


Figure 3.5: UE antenna field pattern gain magnitude at each beam

results of Markov model in Fig. 3.7.

Observation 1. *The throughput decreases in successive step of slot after receiving RS. Furthermore, system throughput decreases with increasing number of schedulable time.*

From (3.1), the transmission rate in transition to lower CQI will be eliminated. Transition probability from simulation extraction shows that there is larger probability of transition to lower CQI than transition to higher or remaining in the same CQI in channel. Therefore, the throughput decreases in successive step of slot and larger schedulable time leads to lower system throughput.

Fig. 3.8 demonstrates the system throughput of simulation results in different UE velocity. Each component of throughput is clarify in Fig 3.9, where UEs velocity is fixed as 10 km/hr.

Table 3.2: MCS feedback table

CQI Index	SNR threshold with 10% BLER (dB)
0	out of range
1	-9.478
2	-6.658
3	-4.098
4	-1.798
5	0.399
6	2.424
7	4.489
8	6.367
9	8.456
10	10.266
11	12.218
12	14.122
13	15.849
14	17.786
15	19.809

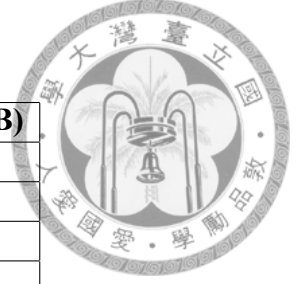


Table 3.3: Channel Model Related Parameters

Model	Description	Parameter values
Omnidirectional path loss (PL) [dB]	$PL = \alpha + 10\beta \log_{10}(d)$	$\alpha = 72.0, \beta = 2.92, d$ is distance in meters
Log-normal shadow fading (X_σ)	$X_\sigma \sim \mathcal{N}(0, \sigma^2)$	$\sigma = 8.7$ dB
Number of clusters (N)	constant	$N = 2$
Number of subpath (M)	constant	$M = 20$
Number of scatters (S)	constant	$S = 2$
BS horizontal cluster central AoD (θ)	Uniform Distribution	$\theta \sim \mathbb{U}(0, 2\pi)$
UE horizontal cluster central AoA (ϕ)	Uniform Distribution	$\phi \sim \mathbb{U}(0, 2\pi)$

Observation 2. *The throughput decreases as UE velocity increase.*

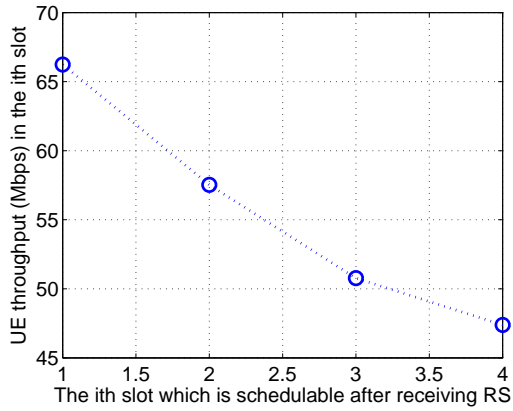
Fig 3.6 and Fig 3.9 can be compared to discover that higher UE velocity leads to lower throughput in each slot. Because channel change rapidly in higher UE velocity, there is more probability of transmission fail in higher UE velocity. This result directly leads to system throughput decrease in higher UE velocity.

In real system, the selected CQI of receiving SNR is not merely higher than corresponding SNR threshold with 10% BLER. Actually, the selected CQI of receiving SNR must higher than a SNR offset plus corresponding SNR threshold with 10% BLER. By uti-

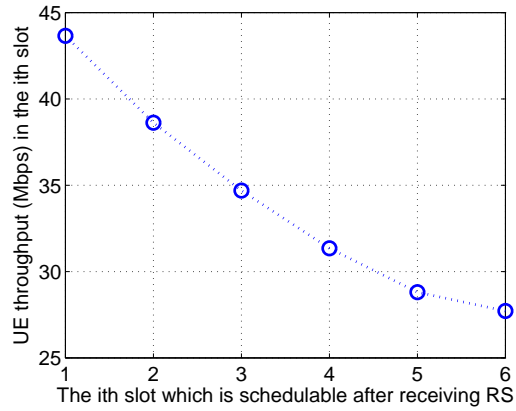
Table 3.4: Other System Parameters



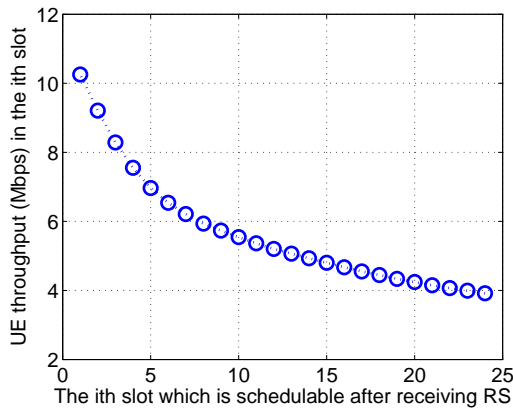
Parameter	Value
BS HPBW	65°
Maximum attenuation of BS antenna pattern	30 dB
UE antenna gain	0 dBi
BS antenna element array	8 × 4 antenna elements
UE antenna element array	4 × 4 antenna elements
BS coverage	maximum distance is $\frac{200}{\sqrt{3}}$ meters
Number of UE in a site	1000 UEs is placed uniformly in BS coverage
UE receiver noise figure	10 dB
Minimum distance between BS and UE	10 m
Number of beamforming direction in a BS sector	8 directions
Number of beamforming direction in a UE	4 directions
Height of BS	18 m
Height of UE	1 m



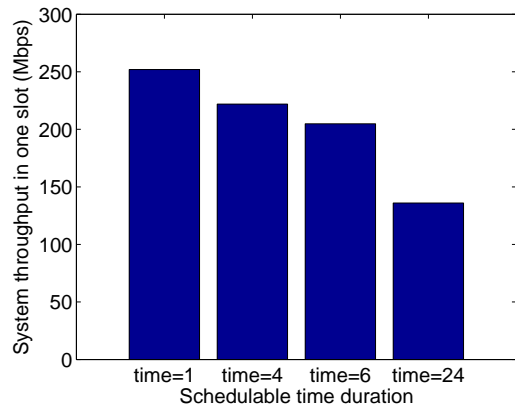
(a) Schedulable time duration = 4 slot, UE velocity = 5 km/hr



(b) Schedulable time duration = 6 slot, UE velocity = 5 km/hr



(c) Schedulable time duration = 24 slot, UE velocity = 5 km/hr



(d) System throughput for each schedulable time duration when UE velocity = 5 km/hr

Figure 3.6: Throughput component in each slot contribute to system throughput for different schedulable time duration

Throughput VS. Schedulable Time when UE Velocity = 5 km/hr

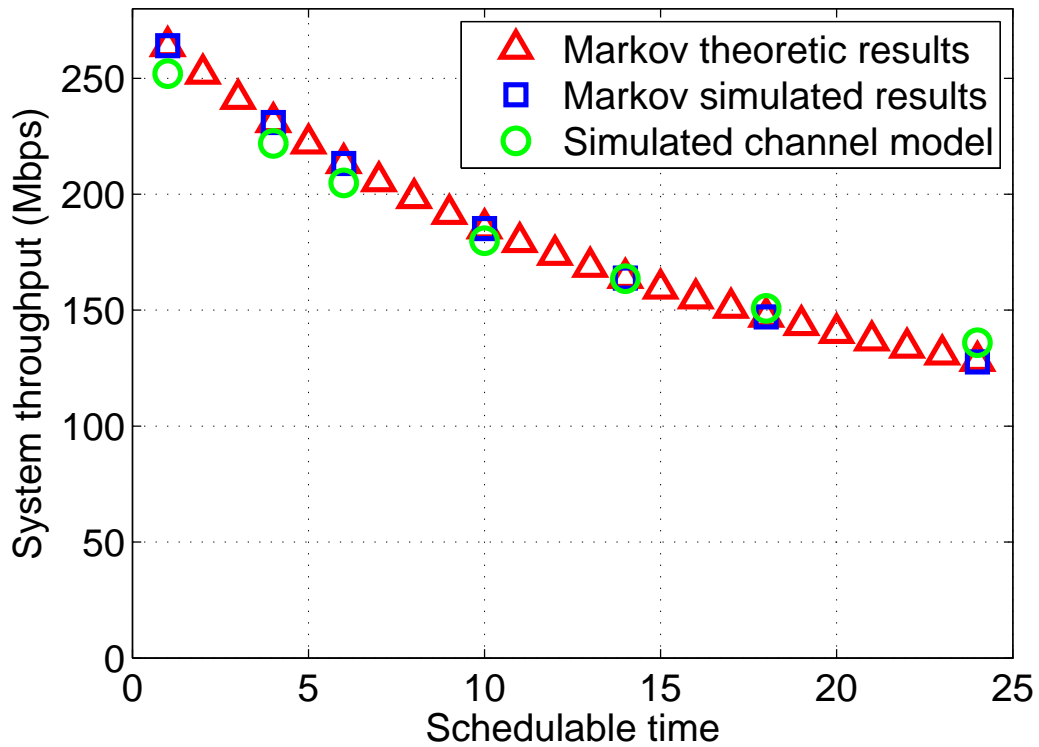


Figure 3.7: Throughput versus schedulable time when UE velocity is 5 km/hr

Throughput VS. UE Velocity

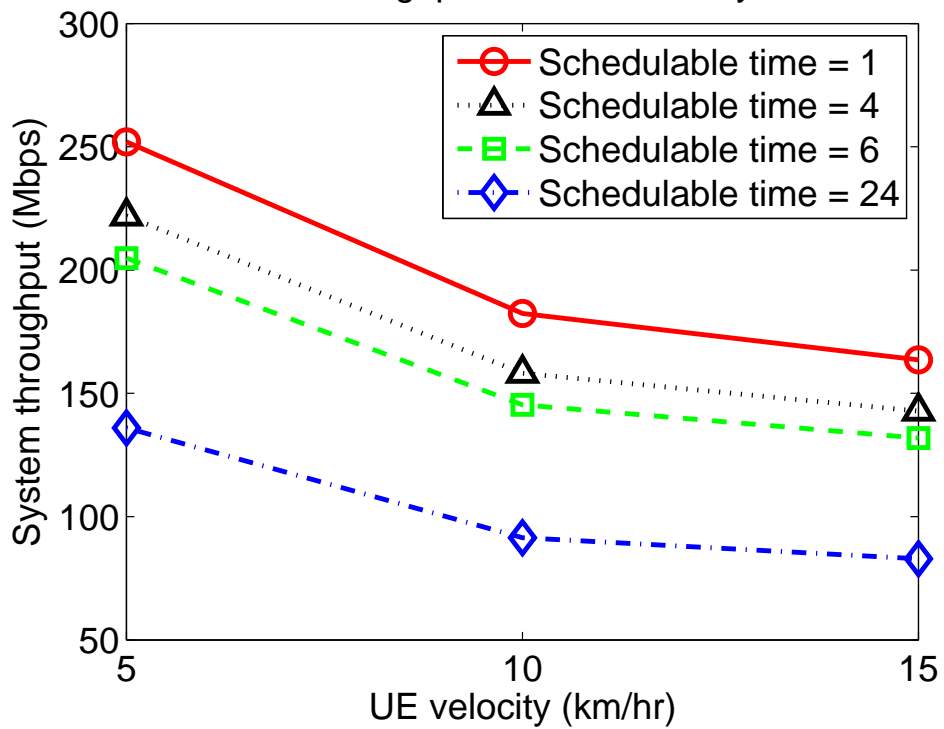
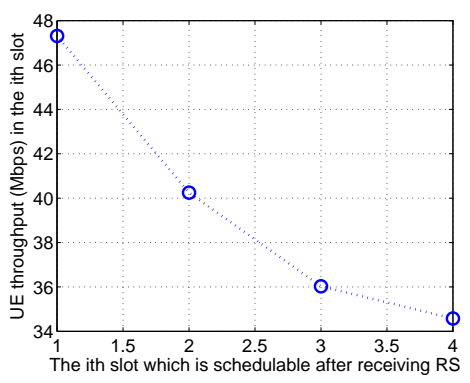
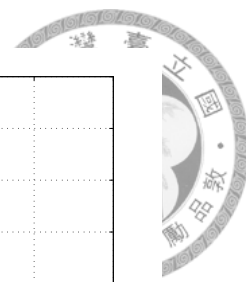
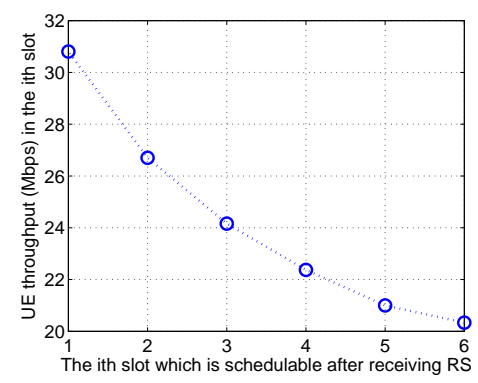


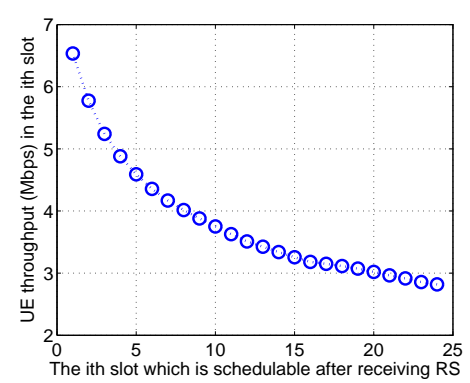
Figure 3.8: Throughput versus UE velocity



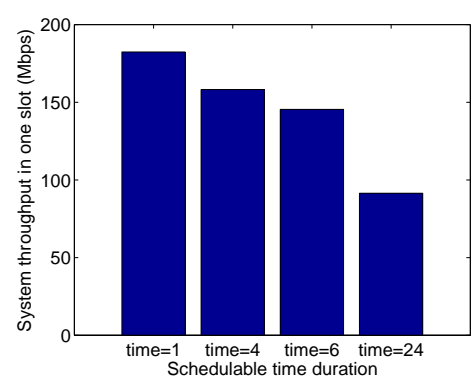
(a) Schedulable time duration = 4 slot, UE velocity = 10 km/hr



(b) Schedulable time duration = 6 slot, UE velocity = 10 km/hr



(c) Schedulable time duration = 24 slot, UE velocity = 10 km/hr



(d) System throughput for each schedulable time duration when UE velocity = 10 km/hr

Figure 3.9: Throughput component in each slot contribute to system throughput for different schedulable time duration

lizing this approach, UE can report a lower CQI to leave a margin for channel variation. In Fig. 3.10 and Fig. 3.11, we study how SNR offset affects our system throughput in different UE velocity. Fig. 3.10 and Fig. 3.11 is simulated under UE velocity 5 km/hr and 10 km/hr respectively. From Fig. 3.10, SNR offset improve system throughput at SNR offset 0.5 and 1.0 dB. However, throughput is not further improved when SNR offset at 1.5 dB. When it comes to UE velocity 10 km/hr in Fig. 3.11, system throughput of schedulable time of 1, 4 and 6 behave in the same trend as which of UE velocity 5 km/hr. However, system throughput of schedulable time of 24 is further improved at 1.5 dB for UE velocity 10 km/hr. We observe that system throughput can be further improved at higher UE velocity. Moreover, system throughput can be further improved at longer schedulable

time.

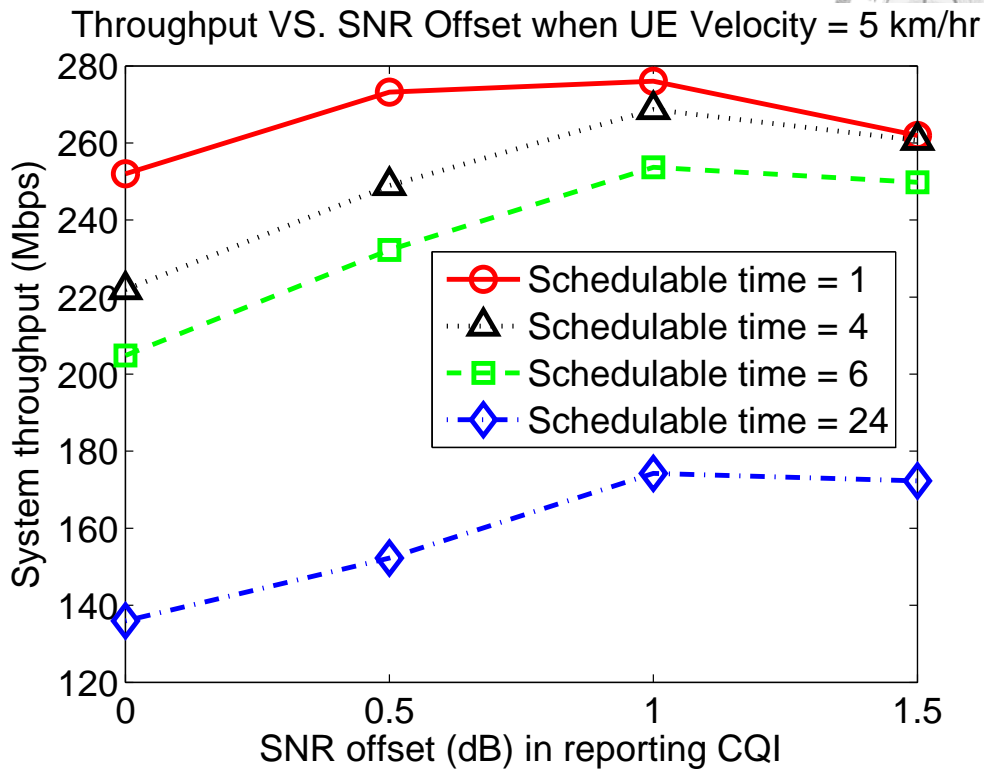


Figure 3.10: Throughput versus SNR offset when UE velocity is 5 km/hr

Observation 3. *Proper SNR offset improves system throughput. Higher UE velocity or longer schedulable time require larger SNR offset*

Higher UE velocity leads to larger channel variation. Larger schedulable time results in larger channel variation in last slot. Therefore, those factors require larger channel margin which leads to larger SNR offset.

3.7 Summary

We propose a desirable scheduling mechanism utilizing directional transmission for 5G mmWave cellular systems. This mechanism is characterized as power-saving and throughput enhancement. We model the system performance using Markov chain and derive theoretic performance which is validated by Markov channel simulation. Simula-

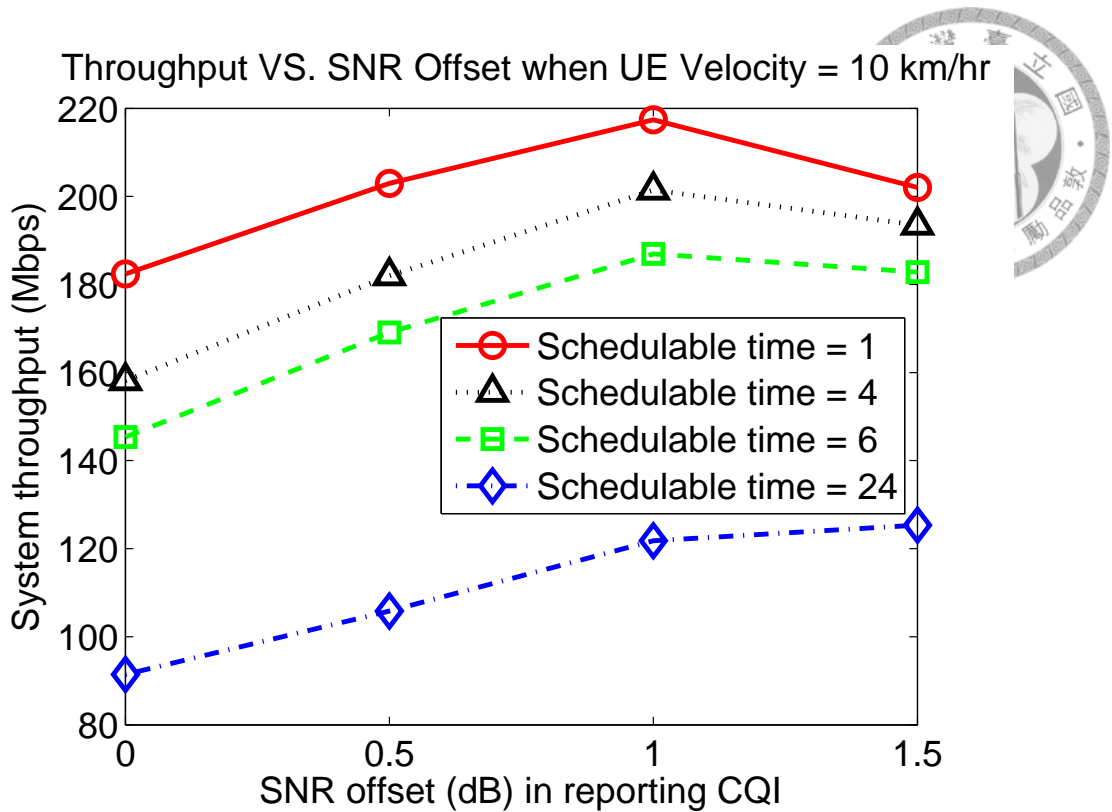


Figure 3.11: Throughput versus SNR offset when UE velocity is 10 km/hr

tion results demonstrate that shorter schedulable time is preferred for higher throughput. However, shorter schedulable time causes that UEs need to wait longer time between each schedulable opportunity. It means longer latency in the system. Furthermore, shorter schedulable time take the risk of idle in BS when no UEs in some beams. UEs which receive less frequently RS can set a longer schedulable time for fairness concern. A scheduling algorithm utilizes this mechanism can be a future work.



Chapter 4

Conclusion

In this dissertation, we propose a reference signal scheme and a scheduling mechanism to take directional RS into account.

In reference signal transmission, we provide a two stages approach to not only boost average reference signal received at each UE but also provide whole RS coverage around BS.


In scheduling mechanism, we introduce dormant behavior to save UE power and take timely throughput into consideration to enhance system throughput. We introduce Markov model to analyze the system and discover shorter schedulable time leads to larger throughput.


Through this two study, we have provided desirable solutions to 5G mmWave cellular network. We believe that these solutions can be applied to boost the performance of future mmWave cellular systems.





Bibliography

- [1] T. S. Rappaport, *et al.* "Millimeter wave mobile communications for 5G cellular: It will work!," *IEEE Access*, vol. 1, pp. 335-349, 2013.
- [2] T. Bai, A. Alkhateeb, and R. W. Heath, "Coverage and Capacity of Millimeter-Wave Cellular Networks," *IEEE Communications Magazine*, vol. 52, no. 9, pp. 70-77, Sept. 2014.
- [3] S. Rangan, T. S. Rappaport, and E. Erkip, "Millimeter-Wave Cellular Wireless Networks: Potentials and Challenges," *Proceedings of the IEEE*, vol. 102, no. 3, pp. 366-385, Mar. 2014.
- [4] H. Shokri-Ghadikolaei, C. Fischione, G. Fodor, P. Popovski, M. Zorzi, "Millimeter wave cellular networks: A MAC layer perspective," *IEEE Transactions on Communications*, vol. 63, no. 10, pp. 3437-3458, Oct. 2015.
- [5] S. Akoum, O. E. Ayach, and R. W. Heath, "Coverage and capacity in mmWave cellular systems," *Conference Record of the Forty Sixth Asilomar Conference on Signals, Systems and Computers (ASILOMAR)*, pp. 688-692, Nov. 2012.
- [6] K. Chandra, A. Doff, Z. Cao, R. V. Prasad, and I. Niemegeers, "60 GHz MAC standardization: Progress and way forward," *12th Annual IEEE Consumer Communications and Networking Conference (CCNC)*, pp. 182-187, Jan. 2015.

- 
- [7] M. Konstantinos, D. M. Z. Estévez, V. Jungnickel, W. Xu, and C. Drewes, “A closed concept for synchronization and cell search in 3GPP LTE systems,” *IEEE Wireless Communications and Networking Conference (WCNC)*, pp. 1-6, April 2009.
- [8] S. Parkvall, *et al.* “LTE-Advanced-Evolving LTE towards IMT-Advanced,” *VTC Fall*, pp. 1-5, Sep. 2008.
- [9] S. Parkvall, A. Furuskar, and E. Dahlman, “Evolution of LTE toward IMT-advanced,” *IEEE Communications Magazine*, vol. 49, no. 2, pp. 84-91, Feb. 2011.
- [10] 3GPP R2-162445, “Radio Link Problem Detection in mmWave System,” TSG-RAN WG2 Meeting, April 2016.
- [11] C. Park, and T. S. Rappaport, “Short-range wireless communications for next-generation networks: UWB, 60 GHz millimeter-wave WPAN, and ZigBee,” *IEEE Wireless Communications*, vol. 14, no. 4, pp.70-78, Aug. 2007.
- [12] J. Wang, *et al.* “Beam codebook based beamforming protocol for multi-Gbps millimeter-wave WPAN systems,” *IEEE Journal on Selected Areas in Communications*, vol. 27, no. 8, pp. 1390-1399, Oct. 2009.
- [13] V. Desai, L. Krzymien, P. Sartori, W. Xiao, A. Soong, and A. Alkhateeb, “Initial beamforming for mmwave communications,” *48th Asilomar Conference on Signals, Systems and Computers*, pp. 1926-1930, Nov. 2014.
- [14] S. Abu-Surra, S. Rajagopal, and X. Zhang, “Synchronization sequence design for mmWave cellular systems.” *IEEE 11th Consumer Communications and Networking Conference*, pp. 617-622, Jan. 2014.

- 
- [15] Shokri-Ghadikolaie Hossein, L. Gkatzikis, C. Fischione, "Beam-searching and transmission scheduling in millimeter wave communications," *IEEE International Conference on Communications (ICC)*, pp. 1292-1297, Jun. 2015.
- [16] B. Li, *et al.* "On the efficient beam-forming training for 60GHz wireless personal area networks," *IEEE Transactions on Wireless Communications*, vol. 12, no. 2, pp. 504-515, Feb. 2013.
- [17] C. Jeong, J. Park, and Hyunkyu Yu. "Random access in millimeter-wave beamforming cellular networks: Issues and approaches." *IEEE Communications Magazine*, vol. 53, no. 1, pp. 180-185, Jan. 2015.
- [18] S. Singh, M. Kulkarni, A. Ghosh, and J. Andrews, "Tractable model for rate in self-backhauled millimeter wave cellular networks," *IEEE Journal on Selected Areas in Communications*, vol. 33, no. 10, pp. 2196-2211, Oct. 2015.
- [19] A. Thornburg and R. W. Heath, "Ergodic capacity in mmWave ad hoc network with imperfect beam alignment," *IEEE Military Communications Conference (MILCOM)*, pp. 1479-1484, Oct. 2015.
- [20] T. Bai and R. W. Heath, "Coverage and rate analysis for millimeter-wave cellular networks," *IEEE Transactions on Wireless Communications*, vol. 14, no. 2, pp. 1100-1114, Feb. 2015.
- [21] C. N. Barati, *et al.* "Directional Cell Discovery in Millimeter Wave Cellular Networks," *IEEE Transactions on Wireless Communications*, vol. 14, no. 12, pp. 6664-6678, Dec. 2015.

- 
- [22] C. N. Barati, *et al.* “Directional Initial Access for Millimeter Wave Cellular Systems”, *arXiv preprint arXiv:1511.06483*, Nov. 2015.
- [23] M. Giordani, M. Mezzavilla, and M. Zorzi, “Initial Access in 5G mm-Wave Cellular Networks,” *arXiv preprint arXiv:1602.07731*, Feb. 2016.
- [24] A. Capone, I. Filippini, and V. Sciancalepore, “Context information for fast cell discovery in mm-wave 5g networks,” *Proceedings of 21st European Wireless Conference*, pp. 1-6. May 2015.
- [25] A. Capone, I. Filippini, V. Sciancalepore, and D. Tremolada, “Obstacle avoidance cell discovery using mm-waves directive antennas in 5G networks,” *IEEE 26th Annual International Symposium on Personal, Indoor, and Mobile Radio Communications (PIMRC)*, pp. 2349-2353, Aug. 2015.
- [26] A. Prasad, *et al.* “Network Assisted Small Cell Discovery in Multi-Layer and mmWave Networks,” *IEEE Conference on Standards for Communication and Networking (CSCN)*, pp. 118-123, Oct. 2015.
- [27] M. R. Akdeniz, *et al.* “Millimeter wave channel modeling and cellular capacity evaluation,” *IEEE Journal on Selected Areas in Communications*, vol. 32, no. 6, pp. 1164-1179, Jun. 2014.
- [28] T. S. Rappaport, G. R. Maccartney, M. K. Samimi, and S. Sun, “Wideband millimeter-wave propagation measurements and channel models for future wireless communication system design,” *IEEE Transactions on Communications*, vol. 63, no. 9, pp. 3029-56, Sep. 2015.

- 
- [29] C. H. Yu, M. P. Chang, and J. C. Guey, "Beam Space Selection for High Rank Millimeter Wave Communication," *81st IEEE Vehicular Technology Conference (VTC Spring)*, pp. 1-5, May 2015.
- [30] 3rd Generation Partnership Project (3GPP), "Evolved Universal Terrestrial Radio Access (E-UTRA); Further advancements for E-UTRA physical layer aspects," Tech. Rep. 3GPP 36.814 (V9.0.0), March 2010.
- [31] J. Fan, Q. Yin, G. Y. Li, B. Peng, and X. Zhu, "MCS selection for throughput improvement in downlink LTE systems," in *Proc. 20th Int. Conf. Comput. Commun. Netw. (ICCCN)*, 2011, pp. 1-5.
- [32] R. Akl, S. Valentin, G. Wunder, and S. Stanczak, "Compensating for CQI aging by channel prediction: The LTE downlink," In *Proc. of IEEE GLOBECOM'12*, 2012, pp. 4821-4827.
- [33] R. Bruno, A. Masaracchia, A. Passarella, "Robust Adaptive Modulation and Coding (AMC) Selection in LTE Systems Using Reinforcement Learning," *IEEE 80th Vehicular Technology Conference Fall*, 2014.
- [34] A. Kuhne, and A. Klein, "Throughput analysis of multi-user OFDMA-systems using imperfect CQI feedback and diversity techniques," *IEEE Journal on Selected Areas in Communications*, vol. 26, no. 8, pp. 1440-1450, Oct. 2008.
- [35] P. Sadeghi, R. Kennedy, P. Rapajic, and R. Shams, "Finite-state Markov modeling of fading channels-a survey of principles and applications," *IEEE Signal Processing Magazine*, vol 25, no. 5, pp. 57-80, Sep. 2008.

[36] Harish Viswanathan, "Capacity of Markov channels with receiver CSI and delayed feedback." *IEEE Transactions on Information Theory*, vol 45, no. 2, pp. 761-771, Mar. 1999.



[37] F. Chen, S. Lijun, C. Meiya, and Y. Dacheng, "A Markov based method for modulation and coding scheme (MCS) with hybrid ARQ retransmission," in *Proc. IFIP International Conference on Wireless and Optical Communications Networks*, pp. 1-5, Apr. 2006.

[38] C. Y. Chen, Y. Y. Chen and H. Y. Wei, "Multi-Cell Interference Coordinated Scheduling in mmWave 5G Cellular Systems," *International Conference on Ubiquitous and Future Networks (ICUFN)*, July. 2016.

[39] 3rd Generation Partnership Project (3GPP), "Spatial Channel Model for Multiple Input Multiple Output (MIMO) simulations," Tech. Rep. 3GPP 25.996 (V13.0.0), Dec. 2015.

[40] J. C. Guey, M. P. Chang, C. H. Yu and C. C. Su, "Modeling and evaluation of beam tracking in mobile millimeter wave communication," *IEEE 26th Annual International Symposium on Personal, Indoor, and Mobile Radio Communications (PIMRC)*, pp. 775-780, 2015.